Molecular Pharmacology Fast Forward. Published on May 15, 2015 as DOI: 10.1124/mol.115.098178
This article has not been copyedited and formatted. The final version may differ from this version.

Identification and characterization of ProTx-III [μ-TRTX-Tp1a], a new voltage-gated sodium channel inhibitor from venom of the tarantula *Thrixopelma pruriens.*

Fernanda C Cardoso, Zoltan Dekan, K. Johan Rosengren, Andelain Erickson, Irina Vetter, Jennifer Deuis, Volker Herzig, Paul Alewood, Glenn F King and Richard J Lewis.

The University of Queensland, Institute for Molecular Bioscience (F.C.C., Z.D., I.V., J.D., V.H., P.A., G.F.K., R.J.L.); School of Biomedical Sciences (K.J.R.); School of Chemistry and Molecular Biosciences (A.E.), Brisbane, QLD 4072, Australia.

Molecular Pharmacology Fast Forward. Published on May 15, 2015 as DOI: 10.1124/mol.115.098178
This article has not been copyedited and formatted. The final version may differ from this version.

Running title: New sodium channel inhibitor from *Thrixopelma pruriens*.

Corresponding authors: Prof. Glenn King and Prof. Richard Lewis, Centre for Pain Research, Institute for Molecular Bioscience, The University of Queensland, 306 Carmody Rd, St Lucia, Brisbane QLD 4072 Australia, Tel: +61 7 3346 2984, E-mail: glenn.king@imb.uq.edu.au and r.lewis@imb.uq.edu.au.

Number of text pages: 34

Number of tables: 3

Number of figures: 11

Number of references: 49

Abstract: 248 words

Introduction: 441 words

Discussion: 997 words

Abbreviations: Ca_V, voltage-gated calcium channel; FLIPR, Fluorescent imaging plate reader; ICK, inhibitor cystine knot; IPTG, Isopropyl β-D-1-thiogalactopyranoside; K_V, voltage-gated potassium channel; nAChR, nicotinic acetylcholine receptor; Na_V, voltage-gated sodium channel; MALDI-TOF, Matrix-assisted laser desorption/ionization time of flight; NMR, Nuclear magnetic resonance; NOESY, Nuclear Overhauser effect spectroscopy; RP-HPLC, reversed-phase high-performance liquid chromatography.

Molecular Pharmacology Fast Forward. Published on May 15, 2015 as DOI: 10.1124/mol.115.098178
This article has not been copyedited and formatted. The final version may differ from this version.

Abstract

Spider venoms are a rich source of ion channel modulators with therapeutic potential. Given the analgesic potential of subtype-selective inhibitors of voltage-gated sodium (Na_V) channels, we screened spider venoms for inhibitors of human $Na_V1.7$ using a high-throughput fluorescent assay. Here, we describe the discovery of a novel $Na_V1.7$ inhibitor, μ-TRTX-Tp1a (Tp1a), isolated from the venom of the Peruvian green-velvet tarantula *Thrixopelma pruriens*. Recombinant and synthetic forms of this 33-residue peptide preferentially inhibited $hNa_v1.7$ > $hNa_v1.6$ > $hNa_v1.2$ > $hNa_v1.1$ > $hNa_v1.3$ channels in fluorescent assays. $Na_V1.7$ inhibition was diminished (IC_{50} 11.5 nM), and the association rate decreased, for the C-terminal acid form of Tp1a compared to the native amidated form (IC_{50} 2.1 nM), suggesting that the peptide C-terminus contributes to its interaction with $hNa_V1.7$. Tp1a had no effect on human voltage-gated calcium channels or nicotinic acetylcholine receptors at 5 μM. Unlike most spider toxins that modulate Na_V channels, Tp1a inhibited $hNa_v1.7$ without significantly altering the voltage-dependence of activation or inactivation. Tp1a proved to be analgesic by reversing spontaneous pain induced in mice by intraplantar injection in OD1, a scorpion toxin that potentiates $hNa_v1.7$. The structure of Tp1a as determined using NMR spectroscopy revealed a classical inhibitor cystine knot motif (ICK). The molecular surface of Tp1a presents a hydrophobic patch surrounded by positively charged residues, with subtle differences to other ICK spider toxins that might contribute to its different pharmacological profile. Tp1a may help guide the development of more selective and potent $hNa_V1.7$ inhibitors for treatment of chronic pain.

Molecular Pharmacology Fast Forward. Published on May 15, 2015 as DOI: 10.1124/mol.115.098178
This article has not been copyedited and formatted. The final version may differ from this version.

Introduction

Voltage-gated sodium (Na_V) channels are transmembrane proteins that underlie action potentials in excitable cells where they contribute to a broad range of vital biological processes (Diss et al., 2004). The Na_V channel superfamily comprises nine subtypes ($Na_V1.1$–$Na_V1.9$) that differ in their primary structure as well as in pharmacological and functional properties. Different subtypes are involved in specialized functions depending on their distribution, biophysical properties and density (Catterall, 2012). These differences provide an opportunity for tissue-specific inhibition of one subtype without affecting the function of others.

Aberrant function and expression of Na_V channels are associated with a range of complex pathological conditions such as chronic pain, epilepsy, and cardiac arrhythmias (Catterall et al., 2010; Remme and Bezzina, 2010; Rogers et al., 2006). Remarkably, individuals with loss-of-function mutations in the gene encoding the pore-forming α-subunit of $hNa_V1.7$ have a complete insensitivity to pain (Cox et al., 2006), with no other sensory deficits except a lack of smell (anosmia) due to the role of $hNa_V1.7$ in olfaction (Rupasinghe et al., 2012; Weiss et al., 2011). Thus, $hNa_v1.7$ has become an exciting, genetically validated target for treating pain disorders (King and Vetter, 2014; Liu and Wood, 2011; Minett et al., 2014).

Spider venoms are a rich source of disulfide-rich peptides with therapeutic potential (King, 2011; Saez et al., 2010). Most of these peptides are ion channel modulators that target a wide range of prey species from invertebrates to mammals (King and Hardy, 2013; Smith et al., 2013). It was recently shown that spider venoms contain at least 12 discrete classes of Na_V channel toxins (NaSpTxs) (Klint et al., 2012) and hence we decided to screen these venoms for specific

Molecular Pharmacology Fast Forward. Published on May 15, 2015 as DOI: 10.1124/mol.115.098178
This article has not been copyedited and formatted. The final version may differ from this version.

inhibitors of $hNa_V1.7$ by optimising a high-throughput FLIPR-based screen we recently described for discovering modulators of endogenously expressed $hNa_V1.7$ (Klint et al., 2015; Vetter et al., 2012). By selectively activating $hNa_v1.7$ using the small-molecule agonist veratridine in combination with the $Na_V1.6/Na_V1.7$-selevtive potentiator OD1, a scorpion-venom peptide (Durek et al., 2013; Jalali et al., 2005; Maertens et al., 2006; Vetter et al., 2012), we were able to directly screen for $hNa_v1.7$ inhibitors. This assay is coupled to calcium influx, allowing high-throughput screens for molecules that inhibit $hNa_v1.7$ using calcium-sensitive fluorescent dyes.

Here we describe the identification of a potent $hNa_v1.7$ inhibitor from venom of the tarantula *Thrixopelma pruriens*. This 33-residue peptide, named μ-TRTX-Tp1a (hereafter Tp1a) on the basis of the rational nomenclature for spider toxins (King et al., 2008), was produced by bacterial expression and chemical synthesis and its Na_V subtype selectivity determined using fluorescent imaging and electrophysiology. We show that that Tp1a is analgesic *in vivo* and reveal its 3D structure as determined using NMR.

Material and methods

Animals. For behavioural assessment, adult male C57BL/6J mice aged 6–8 weeks and weighing 20–25 g were used. Mice were housed in groups of 3 or 4 per cage, under 12 h light-dark cycle, with standard rodent chow and water provided *ad libitum.*

Ethics Statement. Ethical approval for *in vivo* experiments was obtained from The University of Queensland animal ethics committee. Experiments involving animals were conducted in accordance with the Animal Care and Protection Regulation Qld (2012), the *Australian Code of*

Molecular Pharmacology Fast Forward. Published on May 15, 2015 as DOI: 10.1124/mol.115.098178
This article has not been copyedited and formatted. The final version may differ from this version.

Practice for the Care and Use of Animals for Scientific Purposes, 8th edition (2013) and the *International Association for the Study of Pain Guidelines for the Use of Animals in Research*.

Spider venoms. Venoms obtained from 40 species of theraphosid spiders by cheliceral electrostimulation were kept frozen at –20°C before being lyophilized (Herzig and Hodgson, 2009).

Cell culture. Cell culture reagents were from Gibco (Life Technologies Corporation, CA, USA), unless otherwise stated. The human neuroblastoma cell line SH-SY5Y was maintained at 37°C in a humidified 5% CO_2 incubator in Roswell Park Memorial Institute (RPMI) medium supplemented with 15% FBS and 2 mM L-glutamine. Chinese hamster ovarian (CHO) cells expressing recombinant hNa_V channels (EZ cells, ChanTest Corp, OH, USA) were maintained at 37°C in a humidified 5% CO_2 incubator in F-12 medium supplemented with 10% FBS, 100 U/ml penicillin and 100 μg/ml streptomycin. Human Embryonic Kidney (HEK 293) cells expressing recombinant hNa_V subtypes co-expressed with the β1 subunit (SB Drug Discovery, Glasgow, UK) were maintained at 37°C in a humidified 5% CO_2 incubator in Minimal Essential medium (MEM) (Sigma-Aldrich, MO, USA) supplemented with 10% FBS, 100 U/ml penicillin and 100 μg/ml streptomycin, 2 mM L-glutamine and variable concentrations of blasticidin, geneticin and zeocin according to manufacturer's protocol. A tetrodotoxin-resistant (TTX-R) rat $Na_V1.6$ cell line was kindly provided by Prof. Steven Waxman (Yale School of Medicine, CT, USA), and cultured in DMEM supplemented with 10% FBS and 500 μg/ml geneticin. Replicating cells were sub-cultured every 3–4 days in a ratio 1:5 using 0.25% trypsin/EDTA.

Venoms screens against $hNa_v1.7$. Venoms previously identified to inhibit SH-SY5Y cell

Molecular Pharmacology Fast Forward. Published on May 15, 2015 as DOI: 10.1124/mol.115.098178
This article has not been copyedited and formatted. The final version may differ from this version.

responses stimulated non-specifically with veratridine (Klint et al., 2015) were re-screened for $hNa_V1.7$ inhibition as previously described (Vetter et al., 2012). Briefly, SH-SY5Y cells were plated at 40,000 cells per well in 384-well flat clear-bottom black plates (Corning, NY, USA) and cultured at 37°C in a humidified 5% CO_2 incubator for 48 h. Cells were loaded with 20 µl/well Calcium 4 dye (Molecular Devices, CA, USA) reconstituted in assay buffer containing (in mM) 140 NaCl, 11.5 glucose, 5.9 KCl, 1.4 $MgCl_2$, 1.2 NaH_2PO_4, 5 $NaHCO_3$, 1.8 $CaCl_2$ and 10 HEPES pH 7.4 and incubated for 30 min at 37°C in a humidified 5% CO_2 incubator. Fluorescence responses were recorded using excitation of 470–495 nm and emission of 515–575 nm for 10 s to set the baseline, then again 600 s after addition of 10, 1 or 0.1 µg venom/well and for a further 300 s after co-addition of 3 µM veratridine and 30 nM OD1.

Venom peptide purification. Venom from *Thrixopelma pruriens* (1 mg) was dissolved in 100 µl Milli-Q water containing 0.05% trifluoroacetic acid (TFA) (Auspep, VIC, Australia) and 5% acetonitrile (ACN) (Sigma-Aldrich, MO, USA) and centrifuged at 14,000 rpm for 10 min to remove particulates. Venom was fractionated on a C18 reversed-phase (RP) HPLC column (Jupiter 250 x 4.6 mm, 5 µm; Phenomenex, CA, USA) using a gradient established in Milli-Q water containing 0.05% TFA (solvent A) and 90% ACN in 0.043% TFA (solvent B). Fractionation was achieved using the following gradient: 5% B for 5 min, followed by 5–20% B over 5 min then 20–50% B over 70 min at a flow rate of 1 ml/min. Peaks were collected by monitoring the absorbance at 214 nm and fractions lyophilized before storage at –20°C.

Mass spectrometry and sequencing. Peptide masses were determined by matrix-assisted laser desorption/ionization time of flight mass spectrometry (MALDI-TOF MS) using a 4700

Molecular Pharmacology Fast Forward. Published on May 15, 2015 as DOI: 10.1124/mol.115.098178
This article has not been copyedited and formatted. The final version may differ from this version.

Proteomics Bioanalyser Model (Applied Biosystems, CA, USA). Peptides dissolved in water were mixed 1:1 (v/v) with α-cyano-4-hydroxy-cinnamic acid matrix (7 mg/ml in 50% acetonitrile) and mass spectra acquired in positive reflector mode. Reported masses are for the monoisotopic $M+H^+$ ions. C-terminal amidation was determined by electrospray mass spectrometry performed using an AB Sciex Triple TOF 5600 system coupled to a DGU-20AD Nano HPLC (Shimadzu, Kyoto, Japan). For analysis, native Tp1a was reconstituted in 0.1% formic acid and loaded into the HPLC, and data analyzed using Analyst® TF 1.6 software (AB Sciex, MA, USA). N-terminal sequencing was performed by the Australian Proteome Analysis Facility (Sydney, NSW, Australia). Briefly, for N-terminal sequencing the peptide was dissolved in urea (4 M) in ammonium bicarbonate (50 mM) and reduced with dithiothreitol (100 mM) at 56°C for 1 h under argon. The sample was then alkylated using acrylamide (220 mM) for 0.5 h in the dark. The reaction was quenched by the addition of excess dithiothreitol. After desalting by RP-HPLC, the collected fraction was loaded onto pre-cycled bioprene discs and subjected to 31 cycles of Edman N-terminal sequencing using a 494 Procise Protein Sequencing System (Applied Biosystems, CA, USA). For amino acids analysis, samples were reconstituted in 150 µl 20% acetonitrile/0.1% TFA and dried for hydrolysis. For high-sensitivity amino acid analysis, samples underwent 24 h gas phase hydrolysis in 6 M HCl at 110° C. The amount of Asn/Asp and Gln/Glu are reported as the sum of the related amino acids. Cysteine and tryptophan are not analyzed using this method. After hydrolysis, amino acids were analyzed using the Water AccQTag Ultra chemistry on a Waters Acquity UPLC (Waters Corporation, MA, USA).

Recombinant production. A synthetic gene encoding Tp1a, with codons optimized for expression in *Escherichia coli*, was produced and cloned into the pLicC vector by GeneArt (Life

Molecular Pharmacology Fast Forward. Published on May 15, 2015 as DOI: 10.1124/mol.115.098178
This article has not been copyedited and formatted. The final version may differ from this version.

Technologies, CA, USA). This vector contains a MalE signal sequence for periplasmic expression, a His_6 tag for nickel affinity purification, a maltose binding protein (MBP) tag to enhance solubility, and a tobacco etch virus (TEV) protease recognition site preceding the Tp1a gene (Klint et al., 2013). The expression plasmid was transformed in *E. coli* strain BL21(DE3) and cells cultured in Luria-Bertani medium at 37°C 180 rpm. Expression of Tp1a was induced with 0.5 mM IPTG at OD_{600} of 1.2 and cells cultured for further 16 h at 16°C. Cells were harvested by centrifugation for 20 min at 10000 rpm, then the pellet was resuspended in FastBreak lysis buffer (Promega, WI, USA) containing 0.2 mg/ml lysozyme and 10 U/ml DNAse. After 30 min incubation at room temperature, cells were centrifuged for 30 min at 12,000 rpm and the supernatant collected. The fusion protein was captured by passing the lysate through a NI-NTA resin (Sigma-Aldrich, MO, USA) followed by washing with 15 mM imidazole in TN buffer (25 mM Tris, 150 mM NaCl, pH 8). The fusion protein was eluted with 500 mM imidazole in TN buffer, then the eluate was concentrated and desalted against TN buffer using a 30-kDa cut-off Amicon Ultra-15 centrifugal filter (Millipore, MA, USA). Reduced (0.6 mM) and oxidized (0.4 mM) glutathione were added to the sample to facilitate TEV protease cleavage performed with 0.02 mg/ml TEV protease at 30°C for 16 h. The sample was then filtered using a 30-kDa cut-off Amicon Ultra-15 centrifugal filter to remove MBP and uncleaved fusion protein, and then the eluate was loaded onto a C18 column (Vydac 4.6 mm x 250 mm, 5 μm, Grace Discovery Sciences, USA). RP-HPLC was performed using an Ultimate 3000 LC system (Dionex, CA, USA) using a gradient in Milli-Q water/0.05% TFA (solvent A) and 90% ACN/0.045% TFA (solvent B). Peaks were collected, lyophilized and stored at –20°C.

Peptide synthesis. Both the C-terminal amide (Tp1a-NH_2) and acid (Tp1a-OH) forms of Tp1a

Molecular Pharmacology Fast Forward. Published on May 15, 2015 as DOI: 10.1124/mol.115.098178
This article has not been copyedited and formatted. The final version may differ from this version.

were assembled on a Symphony automated peptide synthesizer (Protein Technologies Inc., AZ, USA) using Rink-amide (loading 0.64 mmol/g) or Fmoc-Leu-Wang (loading 0.56 mmol/g) polystyrene resins, respectively, on a 0.1 mmol scale. Fmoc deprotection was achieved using 30% piperidine/DMF. Couplings were performed in DMF using 5 equivalents of Fmoc-amino acid/HBTU/DIEA (1:1:1) relative to resin loading for 2 x 20 min. Amino acid side-chains were protected as follows: Asn(Trt), Asp(OtBu), Cys(Trt), Glu(OtBu), His(Trt), Lys(Boc), Ser(tBu), Trp(Boc). Cleavage from resin and removal of side-chain protecting groups was achieved by treatment with 95% TFA/2.5% TIPS/2.5% H_2O at room temperature (RT) for 2 h. After most of the cleavage solution was evaporated under a stream of N_2, the products were precipitated and washed with cold Et_2O and lyophilised from 50% MeCN/0.1% TFA/H_2O. Tp1a-NH_2: 230 mg; ESI-MS (*m/z*): calc. (avg) 762.7 $[M+5H]^{5+}$, found 762.6. Tp1a-OH: 289 mg; ESI-MS (*m/z*): calc. (avg) 762.9 $[M+5H]^{5+}$, found 762.8. The crude products were purified by preparative HPLC to give 108 and 90 mg of reduced Tp1a-NH_2 and Tp1a-OH, respectively.

Oxidative folding. Purified reduced peptide (50 mg Tp1a-NH_2 or 45 mg Tp1a-OH), reduced glutathione (100 equiv.) and oxidised glutathione (10 equiv.) were dissolved in 6 M GnHCl (21 mL) then added to a solution of 0.36 M NH_4OAc (pH 8.0, 230 mL) and stirred at room temperature with exposure to air for 48 h. The single major products were isolated by preparative HPLC. Tp1a-NH_2: 30 mg; ESI-MS (*m/z*): calc. (avg) 761.5 $[M+5H]^{5+}$, found 761.5. Tp1a-OH: 24.5 mg; ESI-MS (*m/z*): calc. (avg) 761.7 $[M+5H]^{5+}$, found 761.5.

Membrane potential assay. Changes in membrane potential were measured in cells expressing human Na_V subtypes on a FLIPR^{TETRA} using membrane potential dye red (Molecular Devices).

Molecular Pharmacology Fast Forward. Published on May 15, 2015 as DOI: 10.1124/mol.115.098178
This article has not been copyedited and formatted. The final version may differ from this version.

The subtypes hNa$_v$1.1/β1, hNa$_v$1.2/β1, hNa$_v$1.3/β1, hNa$_v$1.4/β1, hNa$_v$1.5/β1, rNa$_v$1.6, hNa$_v$1.7/β1 and hNa$_v$1.8/β1 stably expressed in HEK cells (SB Drug Discovery, Glasgow, UK) were plated at 10,000 cells per well in 384-well flat clear-bottom black plates (Corning, NY, USA) and cultured in complete media at 37°C in a humidified 5% CO_2 incubator for 24 h. For assays, the medium was removed and cells loaded with 20 μl/well of membrane potential dye red reconstituted in assay buffer containing (in mM) 140 NaCl, 11.5 glucose, 5.9 KCl, 1.4 $MgCl_2$, 1.2 NaH_2PO_4, 5 $NaHCO_3$, 1.8 $CaCl_2$. 10 HEPES pH 7.4. Tp1a was added to cells and incubated for 30 min at 37°C in a humidified 5% CO_2 incubator. Changes in membrane potential were recorded using excitation 510–545 nm and emission 565–625 nm for 10 s to set the baseline, then for a further 300 s after addition of 50–70 μM veratridine.

Patch-clamp electrophysiology. Experiments were recorded in recombinant CHO (Chantest) or HEK 293 (SB Drug Discovery) cells expressing specific Na_V subtypes and Na^+ currents measured by using an automated whole-cell patch clamp electrophysiology system (QPatch 16X; Sophion, Denmark). The extracellular solution comprised (in mM) 1 $CaCl_2$, 1 $MgCl_2$, 5 HEPES, 3 KCl, 140 NaCl, 0.1 $CdCl_2$, 20 TEA-Cl at pH 7.3 and 320 mOsm, and the intracellular solution comprised (in mM) 140 CsF, 1/5 EGTA/CsOH, 10 HEPES, 10 NaCl at pH 7.3 and 320 mOsm. The elicited currents were sampled at 25 kHz and filtered at 4 kHz. The average seal, whole-cell and chip resistances values were (in MΩ) 1700, 1672 and 2.1 for CHO cells and 3690, 997 and 2.08 for HEK cells, respectively. Cells with less than 1 nA of peak Na^+ current were not used. Cells were maintained at a holding potential –80 mV and Na^+ currents elicited by 20 ms voltage steps to 0 mV from a –120 mV conditioning pulse applied for 200 ms. For dose-response experiments, cells were incubated for 5 min with increasing concentrations of Tp1a. For on-rate

Molecular Pharmacology Fast Forward. Published on May 15, 2015 as DOI: 10.1124/mol.115.098178
This article has not been copyedited and formatted. The final version may differ from this version.

measurements, Na^+ currents were assessed at 15-s intervals immediately after addition of Tp1a. For off-rate measurements, cells were incubated for 10 min with Tp1a and Na^+ currents assessed at 5-min intervals during saline washes. The K_{on}, K_{off} and K_d where calculated using $K_d = K_{off}/K_{on}$ (nM), where $K_{off} = 1/\tau_{off}$ (s^{-1}) and $K_{on} = (1/\tau_{on}\text{-}K_{off})/[\text{toxin}]$ ($nM^{-1}S^{-1}$). Voltage-activation relationships were obtained by measuring steady-state Na^+ currents elicited by step depolarizations from –110 to +80 mV with 10-mV increments. Peak conductance (G_{Na}) was calculated from $G = I/(V–V_{rev})$, where I, V and V_{rev} represent the current value, membrane potential and reverse potential, respectively. The voltage of steady-state inactivation was estimated using a double-pulse protocol with currents elicited by a 20 ms depolarizing potential of 0 mV following a 500 ms prepulse to potentials from –130 to –10mV using 10-mV increments. Then voltage-dependence of activation and inactivation were determined in the absence or presence of Tp1a (5 min exposure) with the cells before application of the voltage protocols. Experimental data was analyzed using QPatch Assay Software v5.0 (Sophion).

Ca_v1, Ca_v2 and nAChR assays. Ca^{2+} responses were measured using $FLIPR^{TETRA}$ and Calcium 4 dye (Molecular Devices,) using the neuroblastoma cell line SH-SY5Y as previously reported (Sousa et al., 2013; Vetter and Lewis, 2010). SH-SY5Y cells were plated at 40,000 cells per well in 384-well flat clear-bottom black plates (Corning, NY, USA) and cultured at 37°C in a humidified 5% CO_2 incubator 48 h. The medium was removed and cells loaded with 20 µl/well Calcium 4 dye reconstituted in assay buffer containing (in mM) 140 NaCl, 11.5 glucose, 5.9 KCl, 1.4 $MgCl_2$, 1.2 NaH_2PO_4, 5 $NaHCO_3$, 1.8 $CaCl_2$ and 10 HEPES pH 7.4 and incubated for 30 min at 37°C in a humidified 5% CO_2 incubator. For Ca_V1 assays, 1 µM ω-conotoxin CVID ($Ca_V2.2$ blocker) was added to the dye, and for the $Ca_v2.2$ assay 10 µM nifedipine (Ca_V1

Molecular Pharmacology Fast Forward. Published on May 15, 2015 as DOI: 10.1124/mol.115.098178
This article has not been copyedited and formatted. The final version may differ from this version.

blocker) was added to the dye. For assay of the α7 nAChR, 10 μM PNU-120596 (an α7 agonist) was added to the dye. Ca^{2+} fluorescence responses were recorded using excitation 470–495 nm and emission 515–575 nm for 10 s to set the baseline, then again 600 s after addition of 5 μM Tp1a and for a further 300 s after addition of 90 mM $CaCl_2$ for Ca_V, 30 μM choline for the α7 nAChR, or 30 μM nicotine for assay of the α3β2/4 nAChR.

Pain behavioural assessment *in vivo*. Spontaneous pain was induced using OD1, a selective and potent activator of $Na_V1.6$/$Na_V1.7$ (Maertens et al., 2006). OD1 (300 nM) ± rGly-Tp1a (1 μM, 300 nM, 100 nM) in a volume of 40 μL was administered by shallow subcutaneous (intraplantar) injection into the left hindpaw under light isoflurane anaesthesia. Immediately after injection, mice were placed individually into polyvinyl boxes (10 x 10 x 10 cm) and spontaneous pain was quantified by counting the number of paw lifts, licks, shakes, and flinches by a blinded observer over a 40-min period in 5-min intervals from video recordings.

Structure determination of Tp1a. 0.2 mg of either the C-terminal amide or acid form of sTp1a was dissolved in 0.5 ml of 90% H_2O/10% D_2O at pH ~3.5. Two-dimensional homonuclear ^1H NMR data were recorded over the temperature range 15–35˚C at 600 MHz on a Bruker Avance spectrometer equipped with a cryoprobe. Recorded data sets included 2D TOCSY (mixing time 80 ms), 2D NOESY (mixing time 200 ms) and 2D DQF-COSY. Data were recorded with 4K data points in the direct dimension and 512 increments in the indirect dimension over a sweep width of 12 ppm. All data were referenced to the water signal (4.768 ppm at 25˚C).

For structure determination, interproton distances were derived from peak volumes in a NOESY spectrum using automated assignment strategies in the program CYANA (Guntert, 2004). Dihedral-angle restraints were derived from amide-proton coupling constants obtained from 1D

Molecular Pharmacology Fast Forward. Published on May 15, 2015 as DOI: 10.1124/mol.115.098178
This article has not been copyedited and formatted. The final version may differ from this version.

and DQF-COSY spectra. Hydrogen bonds were identified by analysis of amide-proton temperature coefficients (Tc). Amide protons with a Tc > –4.6 ppb/K are likely to be involved in hydrogen bonds (Cierpicki and Otlewski, 2001); for such amides where suitable hydrogen bond acceptors could be identified in preliminary structure calculations, hydrogen-bond restraints were included (Wang et al., 2000). The final family of structures was calculated using the program CNS (Brunger et al., 1998) using protocols from the RECOORD data base (Nederveen et al., 2005) and refinement in explicit water, as described previously (Conibear et al., 2012). From a family of 50 calculated structures, the 20 structures with highest stereochemical quality as judged by MolProbity (Chen et al., 2010) were selected to represent the solution structure of Tp1a. Atomic coordinates and NMR chemical shifts have been submitted to the Protein Data Bank and BioMagResBank, under accession numbers PDB 2mxm and BMRB 25419, respectively.

Data analysis. Curve fitting was achieved using GraphPad Prism Version 6 (GraphPad Software Inc, San Diego, CA, USA) with nonlinear regression with log[inhibitor] versus normalized response and variable Hill slope for dose-responses, Boltzmann sigmoidal equation for voltage-dependence of activation and inactivation analysis and exponential One-phase decay or association for on and off-rate analysis. Data were represented as mean ± SEM from at least *n*=3 replicates. For the *in vivo* experiments, data were presented as mean ± SEM and statistical significance determined by ANOVA with Dunnett's posttest (*n*=4).

RESULTS

Screen for hNa$_v$1.7 inhibitors. Venoms from 40 species of spiders that inhibited veratridine-evoked Na$_V$ channel activity (Klint et al., 2015) were re-screened in an improved assay in which

Molecular Pharmacology Fast Forward. Published on May 15, 2015 as DOI: 10.1124/mol.115.098178
This article has not been copyedited and formatted. The final version may differ from this version.

hNav1.7 was specifically activated using a combination of OD1 and veratridine. Using this approach, 18 spider venoms were found to potently inhibit $hNa_v1.7$ (at least 90% inhibition) at concentrations of 250 and 25 ng/μl (data not shown). The venom of *T. pruriens* potently inhibited $hNa_v1.7$ (Figure 1), consistent with the presence of the previously characterized $hNa_V1.7$ inhibitors ProTx-I and ProTx-II (Middleton et al., 2002). Assay-guided fractionation was used to confirm whether these toxins accounted for the full activity of *T. pruriens* venom.

Peptide toxin identification. Fractionation of *T. pruriens* venom using C18 RP-HPLC revealed five major peaks (Figure 2A), with three fractions inhibiting $hNa_V1.7$ (Figure 2B). The earliest eluting of these peptides, Tp1a, corresponded to the second dominant peak with a retention time of 26.9 min, while the more hydrophobic ProTx-I and ProTx-II eluted at 40.3 and 51.9 min respectively. The reduced hydrophobicity of Tp1a encouraged further studies on this peptide due its potentially more straightforward synthesis. Native Tp1a had a monoisotopic mass of 3799.73 Da as observed by MALDI-TOF and electrospray mass spectrometry (Figure 2C). Edman degradation, tandem mass spectrometry (MS/MS) and amino acid analysis revealed that Tp1a is a 33-residue peptide with a calculated monoisotopic oxidized mass of 3799.70 Da, consistent with the presence of three disulfide bonds and an amidated C-terminus (Figure 3A).

Tp1a belongs to NaSpTx Family 1, a family of spider-venom-derived Na_V channel toxins that comprise 33–35 residues with three disulfide bonds that form a hyperstable ICK motif (Klint et al., 2012). The closest homologs of Tp1a are ω-TRTX-Gr2b (63% identity), β-TRTX-Ps1a (58% identity) and ω-TRTX-Gr2a (58% identity) (Figure 3B). Surprisingly, Tp1a is very dissimilar to ProTx-I (25% identity) and ProTx-II (38% identity) from the same spider, which belongs to

Molecular Pharmacology Fast Forward. Published on May 15, 2015 as DOI: 10.1124/mol.115.098178
This article has not been copyedited and formatted. The final version may differ from this version.

NaSpTx Families 2 and 3, respectively (Klint et al., 2012) (Figure 3C).

Recombinant expression and chemical synthesis of Tp1a. Recombinant Tp1a was produced by periplasmic expression of a MBP-Tp1a fusion protein in *E. coli*. A non-native N-terminal Gly residue was added to facilitate TEV protease cleavage of the fusion protein since this is the preferred residue in the P1' position of the TEV protease recognition site. The MBP-Tp1a fusion protein was purified on a nickel column then TEV cleavage was used to release unfused rGly-Tp1a (Figure 4A). Only 50% of the fusion protein was cleaved, giving a yield of 0.4 mg/L rGly-Tp1a after final purification by RP-HPLC; the observed monoisotopic mass of 3858.23 Da is consistent with the presence of the non-native N-terminal Gly residue (Figure 4B). rGly-Tp1a was produced as a single isomer that eluted on RP-HPLC ~1 min after native Tp1a (nTp1a). The recombinant peptide was lyophilized and stored at 4°C. Chemical synthesis was used to generate the C-terminal amide and acid forms of Tp1a, of which the amidated form coeluted with nTp1a (Figure 5).

Effect of Tp1a on hNa$_v$1.7. Tp1a activity was further investigated by whole-cell patch clamp studies of CHO cells expressing hNa$_v$1.7 (Figure 6). Current traces in the presence and absence of nTp1a, rGly-Tp1a, sTp1a-OH and sTp1a-NH$_2$ are shown in Figure 6A. Native, recombinant and the synthetic C-terminal acid and amide forms of Tp1a inhibited hNa$_V$1.7 with an IC$_{50}$ of 2.1 ± 1.3 (n = 6), 9.5 ± 3.4 (n = 7), 11.5 ± 3.9 (n = 6) and 2.5 ± 0.8 (n = 6) nM, respectively (Figure 6B).

Effect of Tp1a on activation and inactivation of hNa$_v$1.7. Most NaSpTxs are so-called gating

Molecular Pharmacology Fast Forward. Published on May 15, 2015 as DOI: 10.1124/mol.115.098178
This article has not been copyedited and formatted. The final version may differ from this version.

modifiers that modulate Na_V channel activity by modifying the voltage-dependence of activation and/or inactivation (Catterall et al., 2007). Figure 7 shows conductance-voltage and current-voltage relationships in the presence and absence of Tp1a. A Boltzmann sigmoidal fit showed a small shift in the voltage of activation and inactivation to more negative potentials in the presence of nTp1a (-8.89 and -7.24 mV, respectively) and sTp1a-NH_2 (–5.1 mV) (Figure 7A and B). Similar changes in the activation and inactivation of hNa_V1.7 were observed in the presence of sTp1a-OH, with $\Delta V_{1/2}$ shifted –5.27 and –6.52 mV, respectively (Figure 7C). rGly-Tp1a had a more pronounced effect on hNa_V1.7 inactivation, with $\Delta V_{1/2}$ shifted by –13.9 mV, and a lesser effect on activation, with $\Delta V_{1/2}$ shifted –3.3 mV (Figure 7D).

Kinetics of Tp1a inhibition of hNa_v1.7. hNa_v1.7 current inhibition and dissociation constant K_d were estimated following application and washout of Tp1a (Figure 8A-D, Figure 9, Table 1). The association rate (K_{on}) was ~ 10-fold faster for nTp1a and sTp1a-NH_2 compared to sTp1a-OH and rGly-Tp1a at non-saturating concentrations (Figure 8A–D, Table 1). These findings reveal a critical role for the C-terminal functionality in determining the kinetics of Tp1a action on hNa_V1.7. Inhibition of hNa_v1.7 by recombinant and synthetic Tp1a-OH was not completely reversible, with sodium currents recovered to ~60% and ~45% of control levels, respectively (n = 3), after 70 min washout whereas inhibition by native and synthetic Tp1a-NH_2 was quasi-irreversible (n = 3) (Figure 9). The calculated K_{off} values were 3.11 ± 0.2 x 10^{-4} s^{-1} and 3.46 ± 0.5 x 10^{-4} s^{-1} for sTp1a-OH and rGly-Tp1a, respectively (Table 1).

Subtype selectivity of Tp1a. The subtype selectivity of Tp1a was first examined by measuring changes in the membrane potential in HEK293 cells expressing Na_V α subunits co-expressed

Molecular Pharmacology Fast Forward. Published on May 15, 2015 as DOI: 10.1124/mol.115.098178
This article has not been copyedited and formatted. The final version may differ from this version.

with the β1 subunit, except for $Na_V1.6$ which was expressed in the absence of subunits (Table 2). rGly-Tp1a and sTp1a-OH had highest potency for $hNa_V1.7$ (IC_{50} of 1.1 ± 0.13 and 1.5 ± 0.4 μM, respectively), followed by $hNa_V1.2$ = $hNa_V1.1$ > $hNa_V1.6$. No significant activity was observed against $hNa_V1.3$, $hNa_V1.4$, $hNa_V1.5$ or $hNa_V1.8$ at up to 5 μM rTp1a and sTp1a-OH. sTp1a-NH_2 was more potent against all Na_V subtypes, with highest potency against $hNa_V1.7$ (IC_{50} of 0.22 ± 0.05 μM) and $hNa_V1.6$ (IC_{50} of 0.29 ± 0.05 μM) and less potency at $hNa_V1.2$ > $hNa_V1.1$ > $hNa_V1.3$. No activity was observed at $hNa_V1.4$, $hNa_V1.5$ and $hNa_V1.8$ at up to 5 μM sTp1a-NH_2.

Tp1a activity at other Na_V channel subtypes was also investigated using whole cell patch-clamp electrophysiology (Table 2). rGly-Tp1a inhibited $hNa_V1.1$ with IC_{50} of 59.8 ± 26 nM, while sTp1a-OH inhibited this subtype with IC_{50} of 100.9 ± 30 nM. In contrast to the fluorescent assays, rGly-Tp1a and sTp1a-OH were shown to be active at $hNa_v1.3$ by electrophysiology, with IC_{50} values of 21.9 ± 4.02 and 41.3 ± 4.7 nM , respectively. Tp1a-NH_2 was 3.5–9-fold more potent than Tp1a-OH, with IC_{50} values of 11.3 ± 1.2 nM for $hNa_V1.1$ and 11.5 ± 3.0 nM for $hNa_V1.3$. No activity was observed at $hNa_V1.5$ for either rGly-Tp1a or for the acid and amidated forms of sTp1a (in the presence of up to 500 nM). Activity at $hNa_V1.2$, $hNa_V1.4$ and $hNa_V1.8$ were not investigated using electrophysiology.

Effect of Tp1a on Ca_v channels and nAChRs. We investigated the activity of Tp1a on Ca_v channels and nAChRs known to be involved in pain pathways and muscle contraction (Hurst et al., 2013; Zamponi et al., 2009). Tp1a did not affect Ca_V and nAChR activity at concentrations up to 5 μM (data not shown). Currents from these channels were fully inhibited by 10 μM nifedipine for Ca_V1, 1 μM ω-conotoxin CVID for Ca_V2, and 10 μM tubocurarine for the α3β4/2

Molecular Pharmacology Fast Forward. Published on May 15, 2015 as DOI: 10.1124/mol.115.098178
This article has not been copyedited and formatted. The final version may differ from this version.

and α7 nAChRs.

Antinociceptive effects of Tp1a in a mouse model of pain. Intraplantar injection of the $Na_V1.7$ enhancer OD1 in mice led to rapid development of spontaneous pain as evidenced by flinching, lifting, licking and shaking of the affected hindpaw, consistent with the role of $Na_V1.7$ in pain. Intraplantar injection of rGly-Tp1a at 1 μM (40 pmoles in a 40 μl injection) and 300 nM (12 pmoles in a 40 μl injection) significantly reduced spontaneous pain behaviour in a concentration-dependent manner (Figure 10A; OD1, 103 ± 6 flinches/10 min; 1 μM Tp1a, 11 ± 3 flinches/10 min; 300 nM Tp1a, 49 ± 17 flinches/10 min, P <0.05) and this reduction in pain behaviour persisted for 25 min after injection of the highest concentration of Tp1a (Figure 10B).

3D structure of Tp1a. The structure of Tp1a was examined using 2D ^{1}H NMR. Hα chemical shifts, which are sensitive to structural changes (Wishart et al., 1992) indicate that the amidated and acid forms of Tp1a have identical folds, with the only minor differences due to the presence or absence of the proximal C-terminal negative charge (Figure 11A). Thus the difference in pharmacology between these two forms of the peptide is not caused by structural differences.

The 3D structure of the acid form of Tp1a was determined using NMR. The final ensemble of 20 structures is shown in Figures 11B and C and structural statistics are presented in Table 3. The structure is in excellent agreement with the experimental restraints and it has good covalent geometry.

Based on sequence homology we anticipated that Tp1a would adopt an ICK fold. This was confirmed by NMR analysis, which revealed that the peptide contains an ICK motif in which the Cys2-Cys17 and Cys9-Cys22 disulfide bonds form a 14-residue ring that is bisected by the

Molecular Pharmacology Fast Forward. Published on May 15, 2015 as DOI: 10.1124/mol.115.098178
This article has not been copyedited and formatted. The final version may differ from this version.

Cys16-Cys29-XX disulfide bond. Elements of secondary structure include a β-sheet comprising residues 20–23 and 29–31, and several β-turns comprising residues 4–7 and 17–20 (type II), and residues 10–13 and 23-26 (type I). The latter turn is present in the least well defined region of the structure, and based on the significant line broadening observed for His26 it appears at this region is dynamic in solution. In addition to the three disulfide bonds, the structure is stabilized by a large number of hydrogen bonds including both backbone and side-chain groups.

We compared the molecular surface of Tp1a to that of μ-TRTX-Hhn1b and μ-TRTX-Hs2a (Figure 10D). As for Tp1a, μ-TRTX-Hhn1b and μ-TRTX-Hs2a preferentially inhibit $Na_V1.2$, $Na_V1.3$ and $Na_V1.7$, with no effect on $Na_V1.4$ and $Na_V1.5$ (Cai et al., 2014; Xiao et al., 2008). Mutations of μ-TRTX-Hhn1b revealed that Lys27 and Arg29 are critical for activity on Na_V channels (Li et al., 2004), while an alanine scan of μ-TRTX-Hs2a revealed that residues Lys18, Arg26, Lys32 and Trp30 are critical for Na_V channel inhibition (Minassian et al., 2013; Revell et al., 2013). Equivalent residues in the Tp1a structure are Lys8, Arg12 and Lys30, which we propose are likely to be important for Tp1a inhibition of $hNa_v1.7$.

Discussion

Na_V channels have been extensively studied using neurotoxins from spiders, cone snails, centipedes and scorpions that have high affinity and specificity for this class of ion channels (King, 2011). By using an in-house high-throughput screen, we isolated a novel spider-venom peptide (Tp1a) that potently inhibited $hNa_V1.7$ and reversed pain responses *in vivo*.

Isolation and production of Tp1a. Tp1a was identified in the venom of the tarantula *Thrixopelma pruriens* from which the Na_V channel inhibitors ProTx-I and ProTx-II were

Molecular Pharmacology Fast Forward. Published on May 15, 2015 as DOI: 10.1124/mol.115.098178
This article has not been copyedited and formatted. The final version may differ from this version.

previously identified (Middleton et al., 2002). However, despite their common origin, Tp1a has much higher sequence identity with the Na_V channel inhibitors ω-TRTX-Gr2b, β-TRTX-Ps1a and ω-TRTX-Gr2a (Figure 3) than with ProTx-I and ProTx-II. Thus, the venom of *T. pruriens* contains Tp1a from NaSpTx Family 1, ProTx-I from NaSpTx Family 2, and ProTx-II from NaSpTx Family 3, suggesting that Na_V channel inhibition plays a key role in immobilization of prey by this spider.

Recombinant Tp1a was readily produced using a bacterial expression system as reported for other ICK peptides (Klint et al., 2013; Saez et al., 2011), although the recombinant version had a non-native N-terminal Gly residue and the C-terminus was not amidated as in the native toxin. In contrast, chemical synthesis of Tp1a allowed production of both the native amidated form as well as the corresponding free carboxyl form without the extra Gly residue. Cell-based FLIPR assays revealed that both recombinant and synthetic carboxylated Tp1a preferentially inhibited $hNa_V1.7$, while the more potent amidated form preferentially inhibited $hNa_V1.7$ and $hNa_V1.6$ (Table 2). C-terminal amidation also significantly enhanced potency at $hNa_V1.3$ compared to the acid forms of Tp1a.

Pharmacology of Tp1a over Na_v channels. Whole-cell patch clamp electrophysiology was used to further characterize the subtype selectivity of Tp1a. Once again, the amidated form was found to be more potent (Figure 6). Indeed, the potency of amidated Tp1a (IC_{50} 2.1 and 2.5 nM for native and synthetic Tp1a, respectively) is comparable or better than the most potent $hNa_V1.7$ inhibitors described to date, including ProTx-I (IC_{50} 51 nM), ProTx-II (IC_{50} 0.3 nM) and Huwentoxin-IV (IC_{50} 26 nM) as measured using similar approaches (Middleton et al., 2002; Xiao

Molecular Pharmacology Fast Forward. Published on May 15, 2015 as DOI: 10.1124/mol.115.098178
This article has not been copyedited and formatted. The final version may differ from this version.

et al., 2008). Curiously, Tp1a induced no significant changes in the voltage-dependence of activation or steady-state inactivation of $hNa_V1.7$ (Figure 7). This suggests that Tp1a may act like Huwentoxin-IV, which binds to the neurotoxin site 4 located at the extracellular S3-S4 loop of domain II to trap the voltage sensor in a closed configuration (Xiao et al., 2008).

C-terminal amidation increased K_{on} and slowed K_{off} for Tp1a, such that inhibition of $hNa_V1.7$ by amidated Tp1a was quasi-irreversible (Figure 8A-D, Figure 9, Table 1). These kinetic data, the first to be reported for NaSpTx1 Family 1 toxins, support the enhanced potency observed for amidated Tp1a. Amidation of Tp1a enhanced affinity at all targeted subtypes, while the carboxyl form suffered its most dramatic loss of affinity at $hNa_V1.6$ and $hNa_V1.3$. These shifts in potency were observed in both electrophysiology and fluorescent imaging assays, despite the significant differences in the IC_{50} values obtained with the approaches. Such differences in electrophysiology and fluorescent imaging assays for ion channels have been reported previously (Mathes et al., 2009; Terstappen et al., 2010), but the underlying cause remains to be elucidated.

Structure of Tp1a reveals typical ICK motif. The ICK scaffold is the fold adopted by the vast majority of spider-venom peptides (King and Hardy, 2013). The three canonical disulfide bonds in the ICK motif form a knot in which a ring formed by the C1-C4 and C2-C5 disulfide bonds and the intervening sections of polypeptide backbone is penetrated by the third disulfide bridge (C3-C6). ICK peptides differ in the size of the inter-cysteine loops and the length of the N and C-terminal regions, but the ICK motif is expected to provide most of these peptides with high levels of chemical, thermal and biological stability (Saez et al., 2011). As for other members of NaSpTx Family 1, such as hainantoxin-IV [μ-TRTX-Hhn1b] and huwentoxin-IV [μ-TRTX-

Molecular Pharmacology Fast Forward. Published on May 15, 2015 as DOI: 10.1124/mol.115.098178
This article has not been copyedited and formatted. The final version may differ from this version.

Hs2a] (Peng et al., 2002), we found that Tp1a also contains an ICK motif. The β-hairpin loop (i.e., intercystine loop 4) of NaSpTx Family 1 toxins has been identified as an important region for interaction with Na_V channels, and it will be interesting to see whether this is the case for Tp1a. The successful recombinant expression and chemical synthesis of Tp1a demonstrated here will facilitate future studies of structure-activity relationships by enabling rapid and affordable production of Tp1a analogues. Alterations in the C-terminal region can also influence the potency and selectivity of these toxins. These alterations can cause significant structural modifications as reported for huwentoxin-IV, or not affect the structure and still generate striking pharmacological changes (Minassian et al., 2013; Revell et al., 2013). We found that the C-terminus of Tp1a is functionally critical, with C-terminal amidation increasing the potency of the toxin and reducing its reversibility.

Analgesic potential of Tp1a. Given the important role identified for $Na_V1.7$ in nociception, we tested the analgesic efficacy of Tp1a in a rodent pain model model in which nocifensive behaviour (paw lifting, licking and flinching) is elicited by intraplantar administration of the $Na_V1.7$ activator OD1 (Zimmermann et al., 2013). Intraplantar administration of Tp1a reduced the nocifensive behaviour induced by OD1 by ~90%, and this effect persisted up to 25 min after Tp1a administration. This suggests that Tp1a can effectively inhibit $Na_V1.7$ at peripheral sensory nerve endings in the skin. Nonetheless, future detailed assessment of the analgesic potential of Tp1a in more sophisticated disease-specific pain models will provide additional insight into the clinical potential of this peptide for the treatment of chronic pain.

Conclusions: We used a novel high through put screening strategy to rapidly isolate a potent

Molecular Pharmacology Fast Forward. Published on May 15, 2015 as DOI: 10.1124/mol.115.098178
This article has not been copyedited and formatted. The final version may differ from this version.

$Na_v1.7$ inhibitor from spider venom. The pharmacological properties of Tp1a evaluated by fluorescent imaging and electrophysiology approaches revealed crucial role of C-terminal amidation in potency, affinity and Na_v subtype selectivity of spider toxins. Tp1a was analgesic in a Nav1.7 specific model of pain and its well-defined structure may help guide the development of improved $Na_v1.7$ inhibitors.

Acknowledgments

We thank members of the Deutsche Arachnologische Gesellschaft (DeArGe e.V.) for providing spiders, especially Ingo Wendt (Germany) for *T. pruriens*. We thank Dr Alun Jones for help with mass spectrometry, and Niraj Bende and Richard Allen for fractionation of *T. pruriens* venom.

Authorship contributions

Participate in the research design: Cardoso, Lewis and King.

Conducted experiments: Cardoso, Dekan, Rosengren, Erickson, Vetter and Deuis.

Contributed new reagents or analytic tools: Herzig.

Wrote or contributed to the writing of the manuscript: Cardoso, Lewis, King and Alewood.

Molecular Pharmacology Fast Forward. Published on May 15, 2015 as DOI: 10.1124/mol.115.098178
This article has not been copyedited and formatted. The final version may differ from this version.

References

Brunger AT, Adams PD, Clore GM, DeLano WL, Gros P, Grosse-Kunstleve RW, Jiang JS, Kuszewski J, Nilges M, Pannu NS, Read RJ, Rice LM, Simonson T and Warren GL (1998) Crystallography & NMR system: A new software suite for macromolecular structure determination. *Acta Crystallogr D, Biological Crystallography* **54**(5): 905-921.

Cai T, Luo J, Meng E, Ding J, Liang S, Wang S and Liu Z (2014) Mapping the interaction site for the tarantula toxin hainantoxin-IV (beta-TRTX-Hn2a) in the voltage sensor module of domain II of voltage-gated sodium channels. *Peptides* doi: 10.1016/j.peptides.2014.09.005.

Catterall WA (2012) Voltage-gated sodium channels at 60: structure, function and pathophysiology. *J Physiol* **590**(11): 2577-2589.

Catterall WA, Cestele S, Yarov-Yarovoy V, Yu FH, Konoki K and Scheuer T (2007) Voltage-gated ion channels and gating modifier toxins. *Toxicon* **49**(2): 124-141.

Catterall WA, Kalume F and Oakley JC (2010) NaV1.1 channels and epilepsy. *J Physiol* **588**(11): 1849-1859.

Chen VB, Arendall WB, 3rd, Headd JJ, Keedy DA, Immormino RM, Kapral GJ, Murray LW, Richardson JS and Richardson DC (2010) MolProbity: all-atom structure validation for macromolecular crystallography. *Acta crystallogr D, Biological crystallography* **66**(1): 12-21.

Cierpicki T and Otlewski J (2001) Amide proton temperature coefficients as hydrogen bond indicators in proteins. *J Biomol NMR* **21**(3): 249-261.

Conibear AC, Rosengren KJ, Harvey PJ and Craik DJ (2012) Structural characterization of the cyclic cystine ladder motif of theta-defensins. *Biochemistry* **51**(48): 9718-9726.

Cox JJ, Reimann F, Nicholas AK, Thornton G, Roberts E, Springell K, Karbani G, Jafri H, Mannan J, Raashid Y, Al-Gazali L, Hamamy H, Valente EM, Gorman S, Williams R, McHale DP, Wood JN, Gribble FM and Woods CG (2006) An SCN9A channelopathy causes congenital inability to experience pain. *Nature* **444**(7121): 894-898.

Diss JK, Fraser SP and Djamgoz MB (2004) Voltage-gated Na+ channels: multiplicity of expression, plasticity, functional implications and pathophysiological aspects. *Eur Biophys J* **33**(3): 180-193.

Durek T, Vetter I, Wang CI, Motin L, Knapp O, Adams DJ, Lewis RJ and Alewood PF (2013) Chemical engineering and structural and pharmacological characterization of the alpha-scorpion toxin OD1. *ACS Chem Biol* **8**(6): 1215-1222.

Guntert P (2004) Automated NMR structure calculation with CYANA. *Methods Mol Biol* **278**: 353-378.

Herzig V and Hodgson WC (2009) Intersexual variations in the pharmacological properties of Coremiocnemis tropix (Araneae, Theraphosidae) spider venom. *Toxicon* **53**(2): 196-205.

Herzig V, Wood DL, Newell F, Chaumeil PA, Kaas Q, Binford GJ, Nicholson GM, Gorse D and King GF (2011) ArachnoServer 2.0, an updated online resource for spider toxin sequences and structures. *Nucleic Acids Res* **39**: D653-657.

Hurst R, Rollema H and Bertrand D (2013) Nicotinic acetylcholine receptors: from basic science to therapeutics. *Pharmacology & therapeutics* **137**(1): 22-54.

Jalali A, Bosmans F, Amininasab M, Clynen E, Cuypers E, Zaremirakabadi A, Sarbolouki MN, Schoofs L, Vatanpour H and Tytgat J (2005) OD1, the first toxin isolated from the venom

of the scorpion Odonthobuthus doriae active on voltage-gated Na+ channels. *FEBS letters* **579**(19): 4181-4186.

King GF (2011) Venoms as a platform for human drugs: translating toxins into therapeutics. *Expert Opin Biol Ther* **11**(11): 1469-1484.

King GF, Gentz MC, Escoubas P and Nicholson GM (2008) A rational nomenclature for naming peptide toxins from spiders and other venomous animals. *Toxicon* **52**(2): 264-276.

King GF and Hardy MC (2013) Spider-venom peptides: structure, pharmacology, and potential for control of insect pests. *Annu Rev Entomol* **58**: 475-496.

King GF and Vetter I (2014) No gain, no pain: $Na_V1.7$ as an analgesic target. *ACS Chem Neurosci* **5**(9): 749–751.

Klint JK, Senff S, Rupasinghe DB, Er SY, Herzig V, Nicholson GM and King GF (2012) Spider-venom peptides that target voltage-gated sodium channels: pharmacological tools and potential therapeutic leads. *Toxicon* **60**(4): 478-491.

Klint JK, Senff S, Saez NJ, Seshadri R, Lau HY, Bende NS, Undheim EA, Rash LD, Mobli M and King GF (2013) Production of recombinant disulfide-rich venom peptides for structural and functional analysis via expression in the periplasm of *E. coli*. *PloS one* **8**(5): e63865.

Klint JK, Smith JJ, Vetter I, Rupasinghe DB, Er SY, Senff S, Herzig V, Mobli M, Lewis RJ, Bosmans F and King GF (2015) Seven novel modulators of the analgesic target $Na_V1.7$ uncovered using a high-throughput venom-based discovery pipeline. *Br J Pharmacol* **172**(10):2445-2458

Li D, Xiao Y, Xu X, Xiong X, Lu S, Liu Z, Zhu Q, Wang M, Gu X and Liang S (2004) Structure--activity relationships of hainantoxin-IV and structure determination of active and inactive sodium channel blockers. *J Biol Chem* **279**(36): 37734-37740.

Liu M and Wood JN (2011) The roles of sodium channels in nociception: implications for mechanisms of neuropathic pain. *Pain Med* **12 Suppl 3**: S93-99.

Maertens C, Cuypers E, Amininasab M, Jalali A, Vatanpour H and Tytgat J (2006) Potent modulation of the voltage-gated sodium channel $Na_v1.7$ by OD1, a toxin from the scorpion Odonthobuthus doriae. *Mol Pharmacol* **70**(1): 405-414.

Mathes C, Friis S, Finley M and Liu Y (2009) QPatch: the missing link between HTS and ion channel drug discovery. *Comb Chem High throughput Screen* **12**(1): 78-95.

Middleton RE, Warren VA, Kraus RL, Hwang JC, Liu CJ, Dai G, Brochu RM, Kohler MG, Gao YD, Garsky VM, Bogusky MJ, Mehl JT, Cohen CJ and Smith MM (2002) Two tarantula peptides inhibit activation of multiple sodium channels. *Biochemistry* **41**(50): 14734-14747.

Minassian NA, Gibbs A, Shih AY, Liu Y, Neff RA, Sutton SW, Mirzadegan T, Connor J, Fellows R, Husovsky M, Nelson S, Hunter MJ, Flinspach M and Wickenden AD (2013) Analysis of the structural and molecular basis of voltage-sensitive sodium channel inhibition by the spider toxin huwentoxin-IV (μ-TRTX-Hh2a). *J Biol Chem* **288**(31): 22707-22720.

Minett MS, Falk S, Santana-Varela S, Bogdanov YD, Nassar MA, Heegaard AM and Wood JN (2014) Pain without nociceptors? $Na_v1.7$-independent pain mechanisms. *Cell reports* **6**(2): 301-312.

Nederveen AJ, Doreleijers JF, Vranken W, Miller Z, Spronk CA, Nabuurs SB, Guntert P, Livny M, Markley JL, Nilges M, Ulrich EL, Kaptein R and Bonvin AM (2005) RECOORD: a

recalculated coordinate database of 500+ proteins from the PDB using restraints from the BioMagResBank. *Proteins* **59**(4): 662-672.

Peng K, Shu Q, Liu Z and Liang S (2002) Function and solution structure of huwentoxin-IV, a potent neuronal tetrodotoxin (TTX)-sensitive sodium channel antagonist from Chinese bird spider Selenocosmia huwena. *J Biol Chem* **277**(49): 47564-47571.

Remme CA and Bezzina CR (2010) Sodium channel (dys)function and cardiac arrhythmias. *Cardiovasc Ther* **28**(5): 287-294.

Revell JD, Lund PE, Linley JE, Metcalfe J, Burmeister N, Sridharan S, Jones C, Jermutus L and Bednarek MA (2013) Potency optimization of Huwentoxin-IV on hNav1.7: a neurotoxin TTX-S sodium-channel antagonist from the venom of the Chinese bird-eating spider Selenocosmia huwena. *Peptides* **44**: 40-46.

Rogers M, Tang L, Madge DJ and Stevens EB (2006) The role of sodium channels in neuropathic pain. *Semin Cell Dev Biol* **17**(5): 571-581.

Rupasinghe DB, Knapp O, Blomster LV, Schmid AB, Adams DJ, King GF and Ruitenberg MJ (2012) Localization of Nav 1.7 in the normal and injured rodent olfactory system indicates a critical role in olfaction, pheromone sensing and immune function. *Channels* **6**(2): 103-110.

Saez NJ, Mobli M, Bieri M, Chassagnon IR, Malde AK, Gamsjaeger R, Mark AE, Gooley PR, Rash LD and King GF (2011) A dynamic pharmacophore drives the interaction between Psalmotoxin-1 and the putative drug target acid-sensing ion channel 1a. *Mol Pharmacol* **80**(5): 796-808.

Saez NJ, Senff S, Jensen JE, Er SY, Herzig V, Rash LD and King GF (2010) Spider-venom peptides as therapeutics. *Toxins* **2**(12): 2851-2871.

Smith JJ, Herzig V, King GF and Alewood PF (2013) The insecticidal potential of venom peptides. *Cell Mol Life Sci* **70**(19): 3665-3693.

Sousa SR, Vetter I, Ragnarsson L and Lewis RJ (2013) Expression and pharmacology of endogenous Cav channels in SH-SY5Y human neuroblastoma cells. *PloS one* **8**(3): e59293.

Terstappen GC, Roncarati R, Dunlop J and Peri R (2010) Screening technologies for ion channel drug discovery. *Future Med Chem* **2**(5): 715-730.

Vetter I and Lewis RJ (2010) Characterization of endogenous calcium responses in neuronal cell lines. *Biochem Pharmacol* **79**(6): 908-920.

Vetter I, Mozar CA, Durek T, Wingerd JS, Alewood PF, Christie MJ and Lewis RJ (2012) Characterisation of Na(v) types endogenously expressed in human SH-SY5Y neuroblastoma cells. *Biochem Pharmacol* **83**(11): 1562-1571.

Wang X, Connor M, Smith R, Maciejewski MW, Howden ME, Nicholson GM, Christie MJ and King GF (2000) Discovery and characterization of a family of insecticidal neurotoxins with a rare vicinal disulfide bridge. *Nat Struct Biol* **7**(6): 505–513.

Weiss J, Pyrski M, Jacobi E, Bufe B, Willnecker V, Schick B, Zizzari P, Gossage SJ, Greer CA, Leinders-Zufall T, Woods CG, Wood JN and Zufall F (2011) Loss-of-function mutations in sodium channel Nav1.7 cause anosmia. *Nature* **472**(7342): 186–190.

Wishart DS, Sykes BD and Richards FM (1992) The chemical shift index: a fast and simple method for the assignment of protein secondary structure through NMR spectroscopy. *Biochemistry* **31**(6): 1647-1651.

Xiao Y, Bingham JP, Zhu W, Moczydlowski E, Liang S and Cummins TR (2008) Tarantula huwentoxin-IV inhibits neuronal sodium channels by binding to receptor site 4 and

trapping the domain ii voltage sensor in the closed configuration. *J Biol Chem* **283**(40): 27300-27313.

Zamponi GW, Lewis RJ, Todorovic SM, Arneric SP and Snutch TP (2009) Role of voltage-gated calcium channels in ascending pain pathways. *Brain Res Rev* **60**(1): 84-89.

Zimmermann K, Deuis JR, Inserra MC, Collins LS, Namer B, Cabot PJ, Reeh PW, Lewis RJ and Vetter I (2013) Analgesic treatment of ciguatoxin-induced cold allodynia. *Pain* **154**(10): 1999-2006.

Molecular Pharmacology Fast Forward. Published on May 15, 2015 as DOI: 10.1124/mol.115.098178
This article has not been copyedited and formatted. The final version may differ from this version.

Footnotes

This work was supported by the Australian Research Council Discovery Project [Grant DP110103129]; Linkage Project [Grant LP130101143]; Future Fellowships to K.J.R and I.V.; and the Australian National Health & Medical Research Council Principal Research Fellowships to R.J.L., G.F.K., and P.F.A. The Australian Proteome Analysis Facility is supported under the Australian Government's National Collaborative Research Infrastructure Strategy.

Reprint requests

Prof. Richard Lewis, IMB Centre for Pain Research, Institute for Molecular Bioscience, The University of Queensland, 306 Carmody Rd, St Lucia, Brisbane QLD 4072 Australia, Tel: +61 7 3346 2984, E-mail: r.lewis@imb.uq.edu.au.

Molecular Pharmacology Fast Forward. Published on May 15, 2015 as DOI: 10.1124/mol.115.098178
This article has not been copyedited and formatted. The final version may differ from this version.

Figure legends

Figure 1. Screening of *Thrixopelma pruriens* spider venom against $hNa_v1.7$ endogenously expressed in SH-SY5Y cells. Effect of venom from *Thrixopelma pruriens* on $hNa_V1.7$ showing 100% and 90% inhibition at 250 (●) and 25 (+) ng/µl, respectively, and loss of activity at 2.5 ng/µl (⋆). The positive control for $hNa_V1.7$ activation was veratridine plus OD1 (□).

Figure 2. Isolation of novel $hNa_V1.7$ inhibitor from venom of the tarantula *T. pruriens*. (A) RP-HPLC fractionation of crude *T. pruriens* venom (1 mg) on a Phenomenex analytical C18 column using the gradient of solvent B indicated by the dashed line at a flow-rate of 1 ml/min. Fractions were manually collected and screened for $hNa_V1.7$ inhibition. Fractions found to inhibit $hNa_V1.7$ are shaded grey. (B) Effect of RP-HPLC fractions on hNav1.7 activity in SH-SY5Y cells as measured on a FLIPR. Fractions eluting at 26.9, 40.3 and 51.9 min potently inhibited $hNa_V1.7$. The dominant masses found by MALDI-TOF analysis of each of the active fractions are indicated. Masses 3984 and 3823 Da correspond to ProTx-I and ProTx-II, respectively. (C) Analytical RP-HPLC chromatogram and MALDI-TOF mass spectrum of RP-HPLC fraction 12 showing single peak and monoisotopic mass 3779 Da that corresponds to Tp1a peptide.

Figure 3. Determination of sequence of Tp1a and comparison with other spider toxins. (A) Determination of the amino acid sequence of Tp1a. The sequence of the first 31 amino acids was obtained by Edman degradation. The last two amino acids were determined using a combination of tandem mass spectrometry (MS nanospray) and amino acid analysis (AAA). (B) Alignment of Tp1a with spider-venom peptides having at least 40% sequence identity. Identical residues are

Molecular Pharmacology Fast Forward. Published on May 15, 2015 as DOI: 10.1124/mol.115.098178
This article has not been copyedited and formatted. The final version may differ from this version.

shown in bold and cysteines are grey. The percent identity relative to Tp1a and activity reported for each peptide is shown on the far right. Peptide sequences were obtained from the ArachnoServer database (www.arachnoserver.org) (Herzig et al., 2011). Asterisks denote C-terminal amidation. (C) Alignment of the sequence of Tp1a with those of ProTx-I (β/ω-TRTX-Tp1a) and ProTx-II (β/ω-TRTX-Tp2a), two Na_V channel inhibitors previously isolated from the same venom.

Figure 4. Production of recombinant Tp1a. (A) SDS-PAGE gel showing MBP-Tp1a fusion protein purified via nickel affinity chromatography (lane 1) and the efficiency of TEV protease cleavage of the fusion protein (~50%) (lane 2). (B) RP-HPLC purification of cleaved recombinant rGly-Tp1a was performed using a Vydac 218TP C18 column with a two-step gradient of 5–50% solvent B over 45 min followed by 50–80% solvent B over 8 min. MALDI-TOF mass spectrometry yielded a monoisotopic mass of 3857 Da, consistent with the calculated mass for rGly-Tp1a (3857.70).

Figure 5. Comparison of native and synthetic Tp1a. Analytical RP-HPLC chromatograms of native amidated Tp1a (dashed trace), synthetic Tp1a-NH_2 (grey trace), and co-elution of synthetic Tp1a-NH_2 and native Tp1a (black trace). RP-HPLC was performed on a Shimadzu LC20AT system using a Thermo Hypersil GOLD C18 column (2.1 x 100 mm) heated at 40°C. Peptides were eluted using a gradient of 5–50% B over 45 min with a flow rate of 0.3 mL/min.

Figure 6. Inhibition of hNa_V1.7 by Tp1a. (A) Representative records of Na^+ currents before (dashed traces) and after (black traces) addition of 2 nM native and synthetic Tp1a-NH_2 or 10

Molecular Pharmacology Fast Forward. Published on May 15, 2015 as DOI: 10.1124/mol.115.098178
This article has not been copyedited and formatted. The final version may differ from this version.

nM recombinant and synthetic Tp1a-OH. Holding potential was –80 mV. (B) Concentration-response curves for inhibition of $hNa_V1.7$ by native, recombinant, and synthetic acid and amidated Tp1a; the IC_{50} values calculated using I/Imax values and nonlinear regression were 2.1 ± 1.3 (n = 6), 9.5 ± 3.4 (n = 7), 11.5 ± 3.9 (n = 6) and 2.5 ± 0.8 (n = 6) nM (mean ± SD), respectively.

Figure 7. Gating properties of Tp1a. Data (mean ± SD, n = 3) for (A) nTp1a, (B) sTp1a-NH_2, (C) sTp1a-OH and (D) rGly-Tp1a are plotted as G/G_{max} or I/I_{max}. Tp1a had no significant effect on the voltage-dependence of steady-state activation or inactivation. Cells were held at –80 mV. Steady state kinetics were estimated by currents elicited at 10-mV increment steps ranging from –110 to +80 mV. Conductance was calculated using $G = I/(V–V_{rev})$ in which I, V and V_{rev} are the current value, membrane potential and reverse potential, respectively. The voltage-dependence of inactivation was estimated using a double-pulse protocol where currents were elicited by a 20-ms depolarizing potential of 0 mV following a 500 ms prepulse at potentials ranging from –130 to –10 mV with 10-mV increments. The $\Delta V_{1/2}$ for activation and inactivation were -8.89 and -7.24 mV for nTp1a (A), –5.1 and –5.1 mV for sTp1a-NH_2 (B), –5.27 and –6.52 mV for sTp1a-OH (C) and –3.3 and –13.9 mV for rGly-Tp1a (D), respectively.

Figure 8. On-rate of Tp1a inhibition of $hNa_V1.7$. (A–D) Measurement of on-rates for various forms of Tp1a. Na^+ currents were recorded every 15 ms soon after toxin addition. The calculated on-rates were (A) 2.45, 1.63 x 10^3 and 2.01 x 10^3 min for nTp1a at 20, 2 and 0.2 nM, respectively, (B) 2.28, 3.13 x10^3 and 3.49 x 10^3 min for sTp1a-NH_2 at 20, 2 and 0.2 nM, respectively; (C) 2.40, 2.78 x 10^1 and 3.83 x 10^3 min for sTp1a-OH at 150, 15 and 1.5 nM,

Molecular Pharmacology Fast Forward. Published on May 15, 2015 as DOI: 10.1124/mol.115.098178
This article has not been copyedited and formatted. The final version may differ from this version.

respectively; and (D) 3.15, 3.78 x 10^3 and 2.30 x 10^3 min for rGly-Tp1a at 150, 15 and 1.5 nM, respectively.

Figure 9. Off-rate of Tp1a and analogues at hNav1.7. Tp1a was applied at 20 nM for nTp1a and sTp1a-NH_2 and 150 nM for rGly-Tp1a and sTp1a-OH and incubated for 10 min before Na^+ currents were measured every 10 min during saline washout. sTp1a-OH and rGly-Tp1a bound reversibly with off-rates of 53.5 and 47.7 min, respectively, while nTp1a and sTp1a-NH_2 showed quasi-irreversible binding to hNa_V1.7.

Figure 10. Antinociceptive effects of Tp1a. (A) Intraplantar injection of the Na_V1.7 activator OD1 (300 nM) led to rapid development of nocifensive behaviour in mice that slowly declined over 40 min. This spontaneous pain behavior, measured by the number of paw lifts, licks, shakes, and flinches, was significantly attenuated in a concentration dependent manner by co-administration of Tp1a when compared to vehicle control. (B) The reduction in spontaneous pain behaviour persisted for 25 min after injection of the highest concentration of Tp1a (1 μM). Data are presented as mean ± SEM of 3–9 mice/group. Statistical significance was determined by ANOVA with Dunnett's post-test; *$P < 0.05$ compared to control.

Figure 11. 3D structure of Tp1a. (A) Comparison of ^{1}Hα chemical shifts for sTp1a-NH_2 and sTp1a-OH, indicating that C-terminal amidation does not alter the 3D fold of Tp1a. (B) Ensemble of 20 structures chosen to represent the solution structure of Tp1a. Disulfide bonds are shown in yellow. (C) Schematic representation of Tp1a structure showing β-strands (magenta)

Molecular Pharmacology Fast Forward. Published on May 15, 2015 as DOI: 10.1124/mol.115.098178
This article has not been copyedited and formatted. The final version may differ from this version.

and disulfide bonds (yellow). (D) Surface representation of the structures of Tp1a (left), μ-TRTX-Hhn1b (center) and μ-TRTX-Hs2a (right). Positively and negatively charged residues are highlighted in blue and red, respectively. Residues shown to be critical for inhibition of $Na_V1.7$ include K27 and R29 for μ-TRTX-Hhn1b (Li et al., 2004) and K18, R26 and K32 for μ-TRTX-Hs2a (Minassian et al., 2013; Revell et al., 2013).

Molecular Pharmacology Fast Forward. Published on May 15, 2015 as DOI: 10.1124/mol.115.098178
This article has not been copyedited and formatted. The final version may differ from this version.

Table 1. Kinetics of inhibition of $hNa_v1.7$ by nTp1a, sTp1a-NH_2, sTp1a-OH and rGly-Tp1a. Tp1a was applied at 0.2, 2 and 20 nM (nTp1a and sTp1a-NH_2) or 1.5, 15 and 150 nM (sTp1a-OH and rGly-Tp1a) then sodium currents were measured. The kinetics of inhibition and recovery of inhibition were determined from the *I*/*Imax* as function of time from traces shown in Figures 8A–D, fitted to a single exponential fit. Values are from at least three independent experiments (mean ± SD). ND = Not determined.

Toxin	**Concentration**	K_{on}	K_{off}	K_d
	nM	$nM^{-1}s^{-1}$	s^{-1}	*nM*
nTp1a	0.2	$4.1 \pm 1.3 \times 10^{-5}$	0	0
	2.0	$5.1 \pm 2.2 \times 10^{-6}$	0	0
	20	$3.4 \pm 1.7 \times 10^{-4}$	0	0
sTp1a-NH_2	0.2	$2.4 \pm 0.5 \times 10^{-5}$	0	0
	2.0	$2.7 \pm 1.2 \times 10^{-6}$	0	0
	20	$3.6 \pm 0.6 \times 10^{-4}$	0	0
sTp1a-OH	1.5	$2.0 \pm 0.2 \times 10^{-4}$	ND	1.5 ± 0.1
	15	$1.9 \pm 0.4 \times 10^{-5}$	ND	16.2 ± 0.3
	150	$4.4 \pm 1.7 \times 10^{-5}$	$3.1 \pm 0.2 \times 10^{-4}$	7.1 ± 0.5
rGly-Tp1a	1.5	$2.3 \pm 1.3 \times 10^{-4}$	ND	1.5 ± 0.2
	15	$2.3 \pm 0.5 \times 10^{-5}$	ND	15.13 ± 0.03
	150	$2.2 \pm 0.3 \times 10^{-5}$	$3.5 \pm 0.5 \times 10^{-4}$	15.84 ± 0.05

Molecular Pharmacology Fast Forward. Published on May 15, 2015 as DOI: 10.1124/mol.115.098178
This article has not been copyedited and formatted. The final version may differ from this version.

Table 2. Tp1a activity on Na_V channels evaluated by fluorescent imaging and electrophysiology represented as IC_{50} values. For fluorescent assays, hNa_V recombinant cells lines were incubated with rGly-Tp1a, sTp1a-NH_2 or sTp1a-OH for 30 min followed by activation with veratridine/OD1. Fluorescent intensity was normalized against positive and negative controls and maximum response from 5 min reading after Na_V activation used for plotting the concentration-response curves. For electrophysiology assays, Na_V recombinant cell lines held at –80 mV were incubated with rGly-Tp1a, sTp1a-OH or sTp1a- NH_2 for 5 min followed by a pre-pulse of –120 mV for 200 ms and activation with a single pulse of 0 mV for 20 ms. *I*/*I*max values were used for plotting the concentration-response curves. Values are from at least three independent experiments (mean ± SD). ND = Not determined.

Method	**Toxin**	**$hNa_V1.1$**	**$hNa_V1.2$**	**$hNa_V1.3$**	**$hNa_V1.4$**	**$hNa_V1.5$**	**$hNa_V1.6$**	**$hNa_V1.7$**	**$hNa_V1.8$**
Fluorescent imaging assay (μM)	rGly-Tp1a	2.8±1.4	2.4±0.4	13.7±1.0	>5	>5	4.5±1.3	1.12±0.3	>5
	sTp1a-OH	1.5±0.2	1.4±0.7	12.1±5.6	>5	>5	3.7±1.1	1.5±0.4	>5
	sTp1a-NH_2	0.5±0.1	0.3±0.1	0.9±0.2	>5	>5	0.29±0.05	0.22±0.05	>5
Electro physiology (nM)	rGly-Tp1a	60±26	ND	21.9±4.0	ND	>500	ND	9.5±3.4	ND
	sTp1a-OH	101±30	ND	41.3±4.7	ND	>500	ND	11.5±3.9	ND
	sTp1a-NH_2	11.3±1.2	ND	11.5±3.0	ND	>50	ND	2.5±0.8	ND

Molecular Pharmacology Fast Forward. Published on May 15, 2015 as DOI: 10.1124/mol.115.098178
This article has not been copyedited and formatted. The final version may differ from this version.

Table 3. Structural statistics for the ensemble of Tp1a structures.

NMR distance & dihedral statistics	
Distance constraints:	
Total	349
Intra-residual ($\|i-j\| = 0$)	168
Sequential ($\|i-j\| = 1$)	100
Medium range ($\|i-j\| \leq 4$)	36
Long range ($\|i-j\| \geq 5$)	45
Hydrogen bonds (for 12 H-bonds)	24
Dihedral Angles:	
ϕ	19
χ_1	18
Structure statistics	
Violations	
Distance constraints (> 0.2 Å)	0
Dihedral angle constraints (> 2º)	0
Energies (kcal/mol, mean ± standard deviation)	
Overall	–1145 ± 36
Bond	13.4 ± 1.1
Angles	35.7 ± 2.8
Improper	12.4 ± 2.0
vdw	–155.0 ± 5.9
NOE (experimental)	0.068 ± 0.018
cDih (experimental)	0.13 ± 0.15
Dihed	150.6 ± 1.9
Elec	–1202 ± 42
RMS Deviation from idealized geometry	
Bond length (Å)	0.0104 ± 0.00043
Bond angles (º)	1.08 ± 0.98
Impropers (º)	1.07 ± 0.96
Average pairwise root mean square deviation[a] (Å)	
Heavy	1.50 ± 0.30
Backbone	0.73 ± 0.25

Molecular Pharmacology Fast Forward. Published on May 15, 2015 as DOI: 10.1124/mol.115.098178
This article has not been copyedited and formatted. The final version may differ from this version.

MOLPROBITY	
Clash Score, all atoms[b]	5.5 ± 3.2
Poor Rotamers	0.8 ± 0.6
Ramachandran Favoured (%)	98.2 ± 2.3
Ramachandran Allowed (%)	1.93 ± 2.31
Ramachandran Outliers (%)	0 ± 0
Molprobity Score	1.63 ± 0.34
Molprobity Score Percentile[c]	88.2 ± 8.7
Cβ deviations, Bad backbone bonds/angles	0 ± 0

[a]Pairwise root mean square deviation from 20 refined structures over residues 2–29.

[b]Number of steric overlaps (>0.4 Å) per 1000 atoms.

[C]100% is the best among structures of comparable resolution, 0% is the worst.

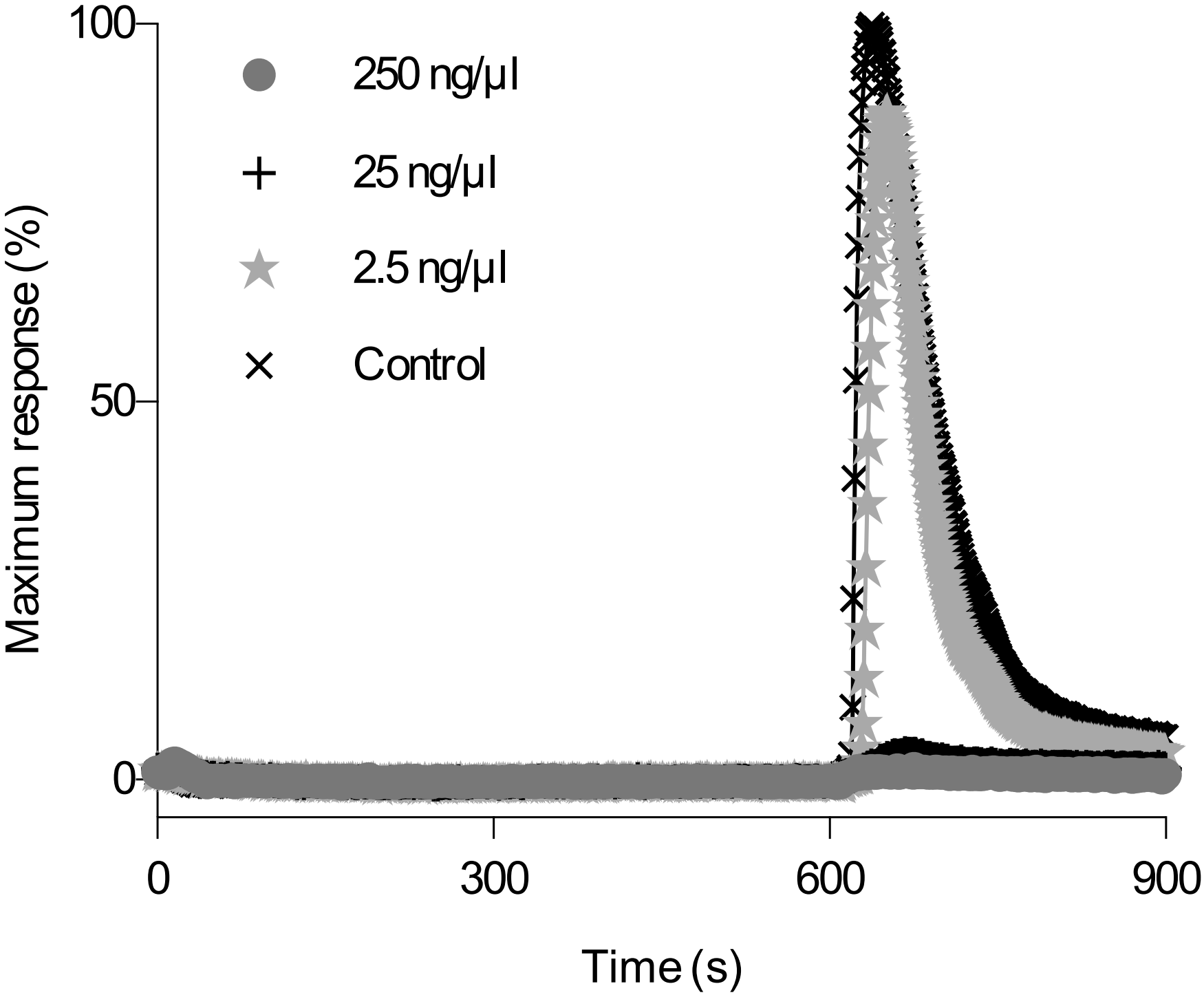
100
50
0
Maximum response (%)
250 ng/µl
25 ng/µl
2.5 ng/µl
Control
0
300
600
900
Time (s)

Figure 1

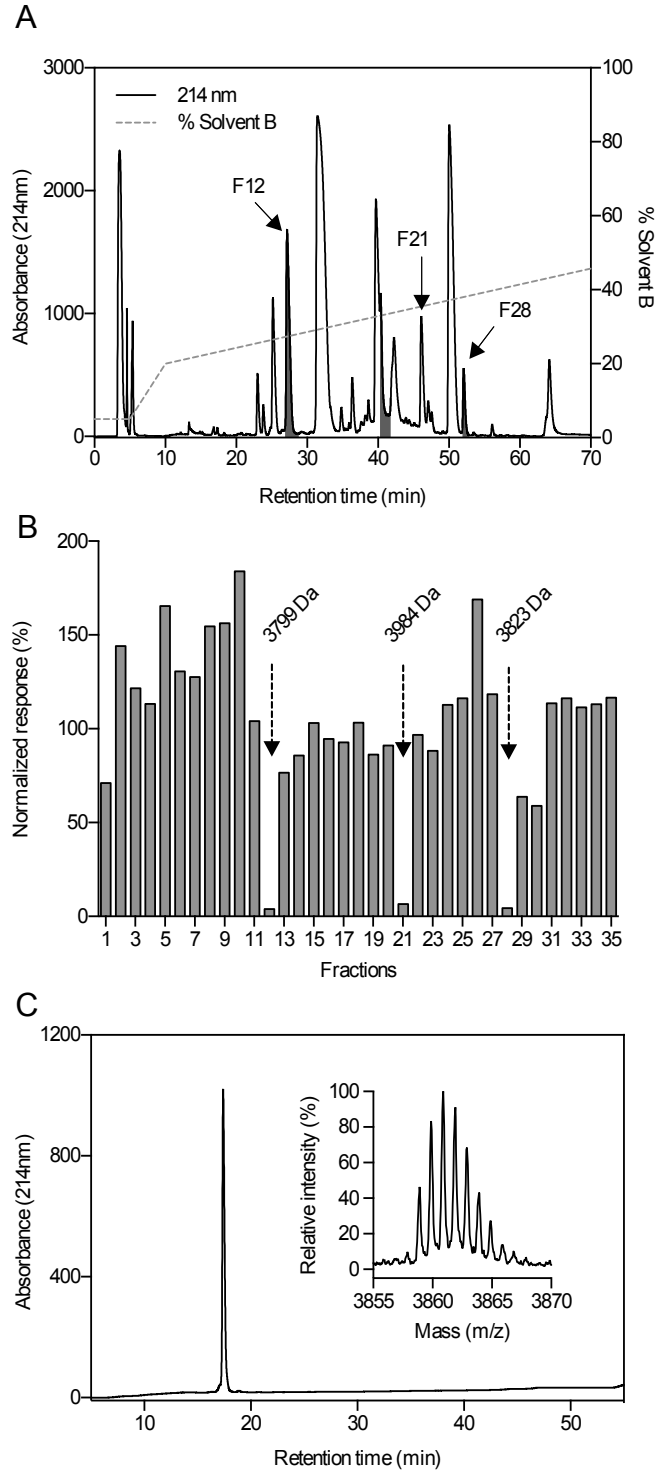
A
214 nm
% Solvent B
F12
F21
F28
Absorbance (214nm)
% Solvent B
Retention time (min)
B
3799 Da
3984 Da
3823 Da
Normalized response (%)
Fractions
C
Absorbance (214nm)
Relative intensity (%)
Mass (m/z)
Retention time (min)

Figure 2

A

Edman sequencing	DCLKFGWKCNPRNDKCCSGLKCGSNHNWCKL
MS nanospray	D----------H(L or I)
AAA	1H,2S, 1R, 3G, 6D/N, 1P, 5K, 1I, 3L, 1F
Final sequence	DCLKFGWKCNPRNDKCCSGLKCGSNHNWCKLHI

B

Toxin name	Sequence		Identity(%)	Activity
μ-TRTX-Tp1a	-**D**C**L**K**FGWK**C**NP**R**N**DK**CCS--**GLK**C**G**S**N**H**N**W**C**K**L**H**I**--	33*	100	Na_v
ω-TRTX-Gr2b	-GC**L**Q**F**M**WK**C**NP**D**N**DK**CCR-PN**LK**CNTY**H**K**W**CEFVT--	34	63	Ca_v
β-TRTX-Ps1a	-**D**C**L**G**FL**W**K**C**NP**S**N**DK**CCR-PN**L**VCSRKDK**W**C**K**YQ**I**--	34	58	Na_v
ω-TRTX-Gr2a	-**D**C**L**G**F**MR**K**C**I**P**D**N**DK**CCR-PNLVCSRT**H**K**W**C**K**YVFGK	36	58	Ca_v, Na_v, K_v
U16-TRTX-Cg1a	D**D**C**L**GMFSSC**NP**D**N**D**K**CCE--**GRK**CDRRDQ**W**C**K**WNPW-	35	56	Unkown
U16-TRTX-Cg1b	D**D**C**L**GLFSSC**NP**D**N**D**K**CCE--**GRK**CNRRDK**W**C**KL**KLW-	35	54	Unknown
μ-TRTX-Hhn1b	-EC**L**G**FG**KGC**NP**S**ND**QCCKSSN**L**VCSRK**H**R**W**C**K**YE**I**--	35*	54	Na_v
κ-TRTX-Gr4b	-**D**C**L**GWFKGC**D**P**D**N**DK**CCE--**G**Y**K**CNRRDK**W**C**K**YKLWK	35	53	K_vAP
κ-TRTX-Gr4a	-**D**C**L**GWFKGC**D**P**D**N**DK**CCE--**G**Y**K**CNRRDK**W**C**K**YKLW-	34	53	K_vAP
U24-TRXT-Cg1a	-**D**C**L**GLF**W**IC**N**YMDD**K**CCP--**G**Y**K**CERSSP**W**C**K**ID**I**WG	35	51	Unkown
μ-TRTX-Hhn1a	-EC**L**G**FG**KGC**NP**S**ND**QCCKSANLVCSRK**H**R**W**C**K**YE**I**--	35	51	Na_v
κ-TRTX-Gr4c	-**D**C**L**GWFKGC**D**P**D**N**DK**CCE--NY**K**CNRRDK**W**C**K**YKLWK	35	50	K_vAP
κ-TRTX-Tb1b	D**D**C**L**GMFSSC**D**P**K**N**DK**CCP--NRVC**R**SRDQ**W**C**K**YKLW-	35	50	K_v4.2
κ-TRTX-Tb1a	AAC**L**GMFESC**D**PN**NDK**CCP--NREC**N**RK**H**K**W**C**K**YKLW-	35	48	K_v4.2
β-TRTX-Cm1a	-**D**C**L**GWFKSC**D**P**K**N**DK**CCK--NYTCSRRDR**W**C**K**YDL--	33*	46	Na_v
β-TRTX-Cm1b	-**D**C**L**GWFKSC**D**P**K**N**DK**CCK--NYTCSRRDR**W**C**K**YYL--	33*	42	Na_v
μ-TRTX-Hhn2a	-GCKG**FG**DSCT**P**GKNECCP--NYACS**S**K**H**K**W**C**K**VYL--	33	40	Na_v

C

μ-TRTX-Tp1a	DCLKFG**W**K**C**NPRND**K**CCS**GL**KCGSNHN**W**C**K**LH-**L**--	33	100	Na_v
β-TRTX-Tp1a	ECRYWLGGCSAGQ-TCCKH**L**VCSRRHG**W**CVWDGTFS	35	25	Na_v,Ca_v3,K_v2
β-TRTX-Tp2a	YCQKWM**W**TCDSER-**K**CC**E**GMVC---RL**W**C**K**KK-**L**W-	30	38	Na_v,Ca_v3

Figure 3

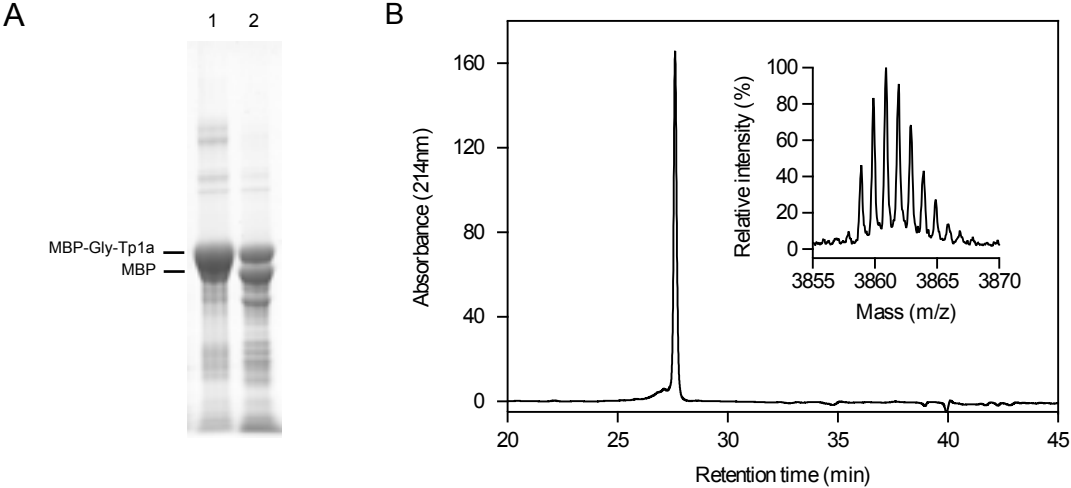
A
1
2
MBP-Gly-Tp1a
MBP
B
Absorbance (214nm)
160
120
80
40
0
20
25
30
35
40
45
Retention time (min)
Relative intensity (%)
100
80
60
40
20
0
3855
3860
3865
3870
Mass (m/z)

Figure 4

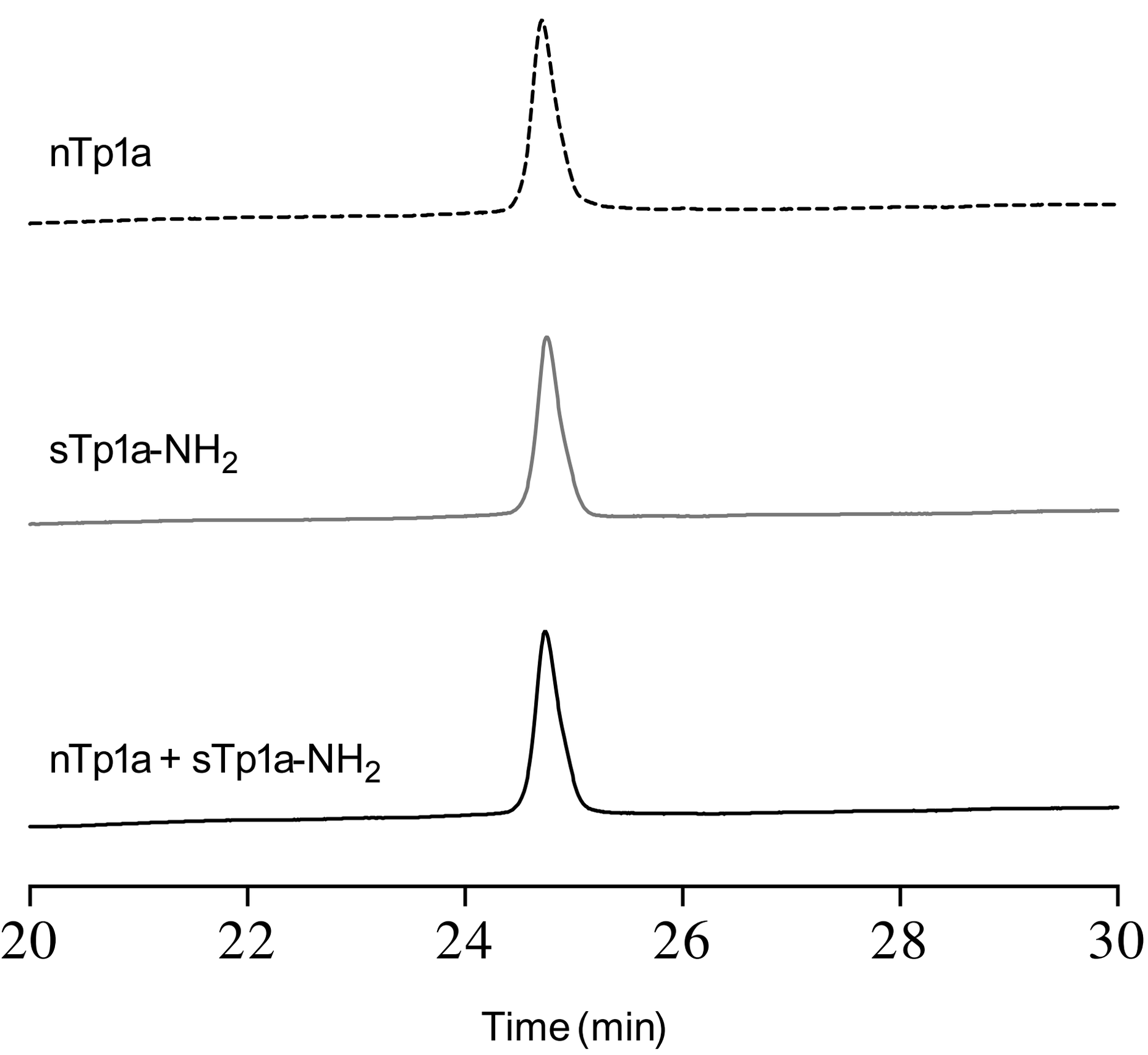

Figure 5

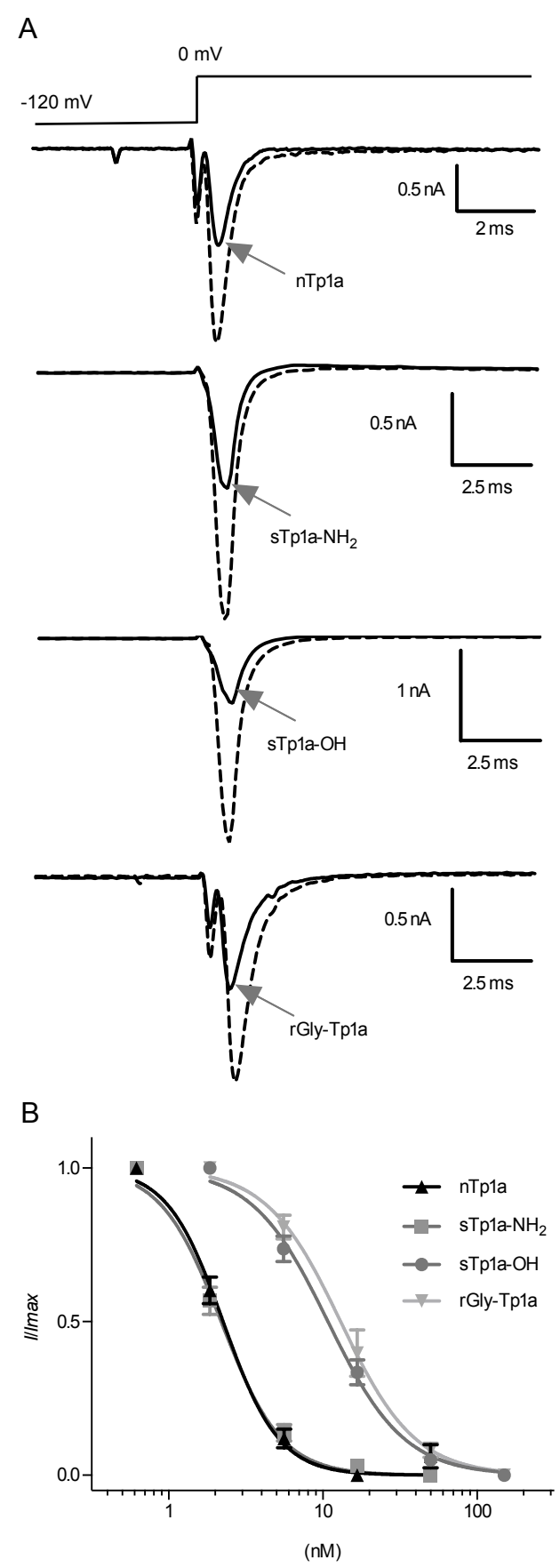
A
0 mV
-120 mV
0.5 nA
2 ms
nTp1a
0.5 nA
2.5 ms
sTp1a-NH2
1 nA
2.5 ms
sTp1a-OH
0.5 nA
2.5 ms
rGly-Tp1a
B
1.0
0.5
0.0
I/Imax
1
10
100
(nM)
nTp1a
sTp1a-NH2
sTp1a-OH
rGly-Tp1a

Figure 6

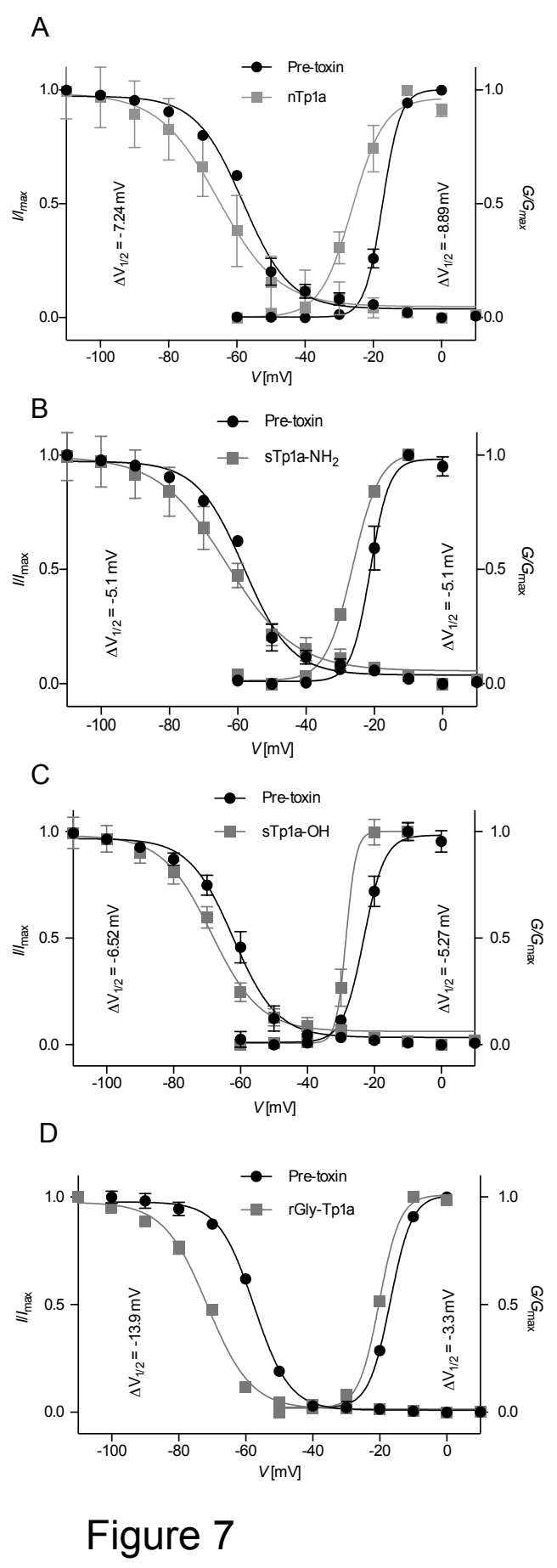
A
Pre-toxin
nTp1a
I/I_{max}
G/G_{max}
$\Delta V_{1/2}$ = -7.24 mV
$\Delta V_{1/2}$ = -8.89 mV
1.0
0.5
0.0
-100
-80
-60
-40
-20
0
V [mV]
B
Pre-toxin
sTp1a-NH$_2$
$\Delta V_{1/2}$ = -5.1 mV
$\Delta V_{1/2}$ = -5.1 mV
C
Pre-toxin
sTp1a-OH
$\Delta V_{1/2}$ = -6.52 mV
$\Delta V_{1/2}$ = -5.27 mV
D
Pre-toxin
rGly-Tp1a
$\Delta V_{1/2}$ = -13.9 mV
$\Delta V_{1/2}$ = -3.3 mV

Figure 7

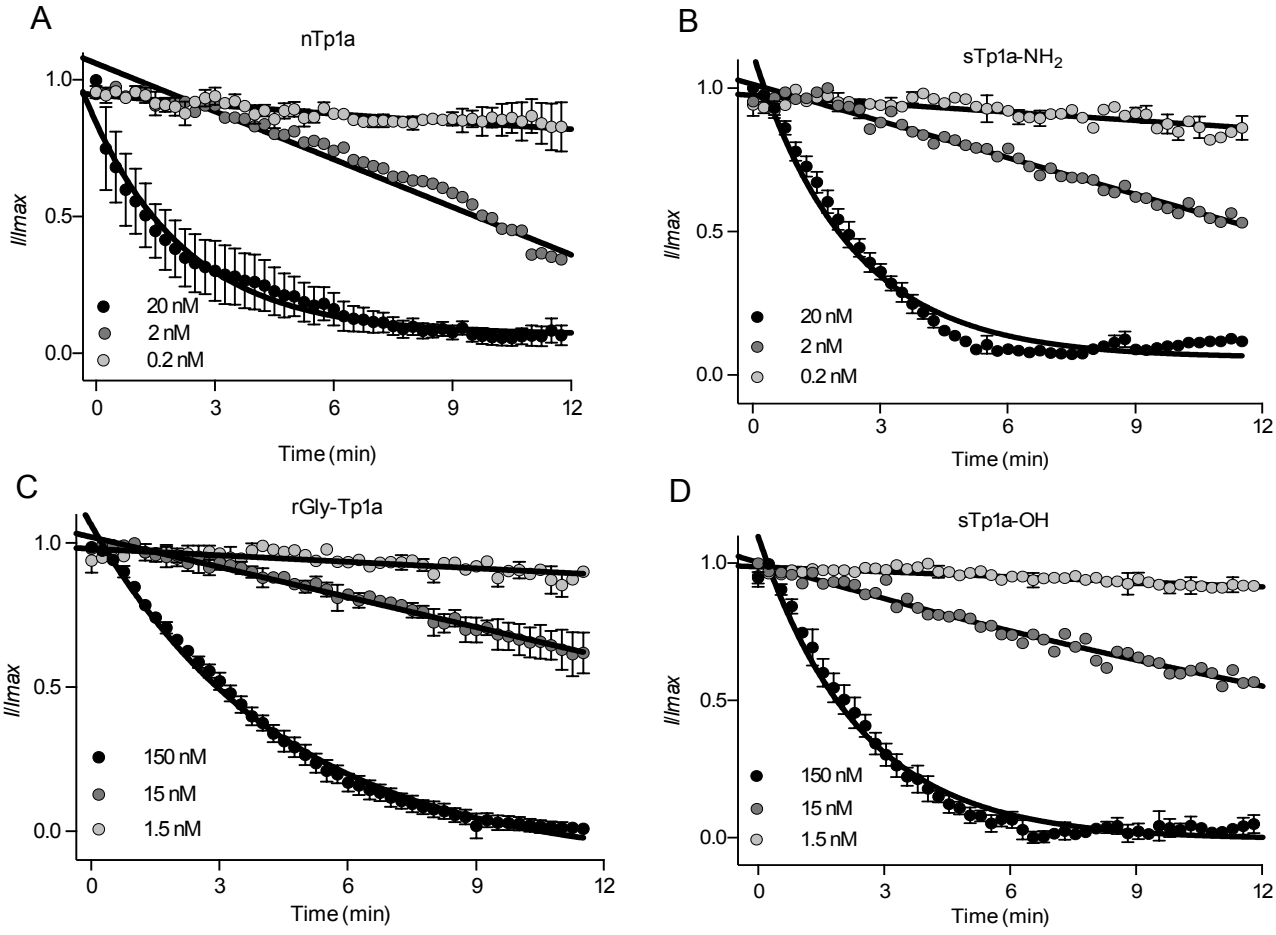
A
nTp1a
I/Imax
1.0
0.5
0.0
20 nM
2 nM
0.2 nM
0
3
6
9
12
Time (min)
B
sTp1a-NH2
I/Imax
1.0
0.5
0.0
20 nM
2 nM
0.2 nM
0
3
6
9
12
Time (min)
C
rGly-Tp1a
I/Imax
1.0
0.5
0.0
150 nM
15 nM
1.5 nM
0
3
6
9
12
Time (min)
D
sTp1a-OH
I/Imax
1.0
0.5
0.0
150 nM
15 nM
1.5 nM
0
3
6
9
12
Time (min)

Figure 8

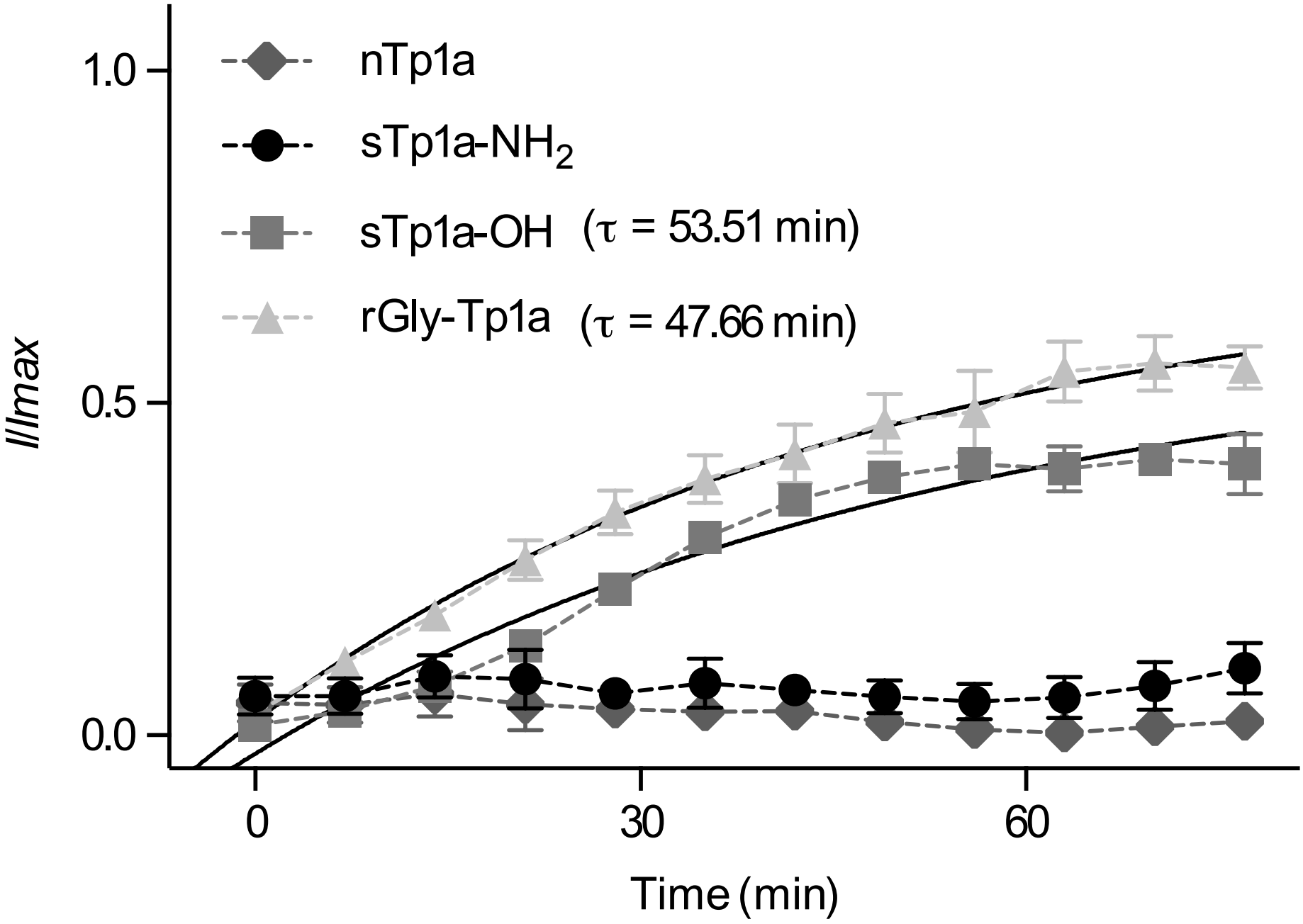
nTp1a
sTp1a-NH2
sTp1a-OH (τ = 53.51 min)
rGly-Tp1a (τ = 47.66 min)
I/Imax
1.0
0.5
0.0
0
30
60
Time (min)

Figure 9

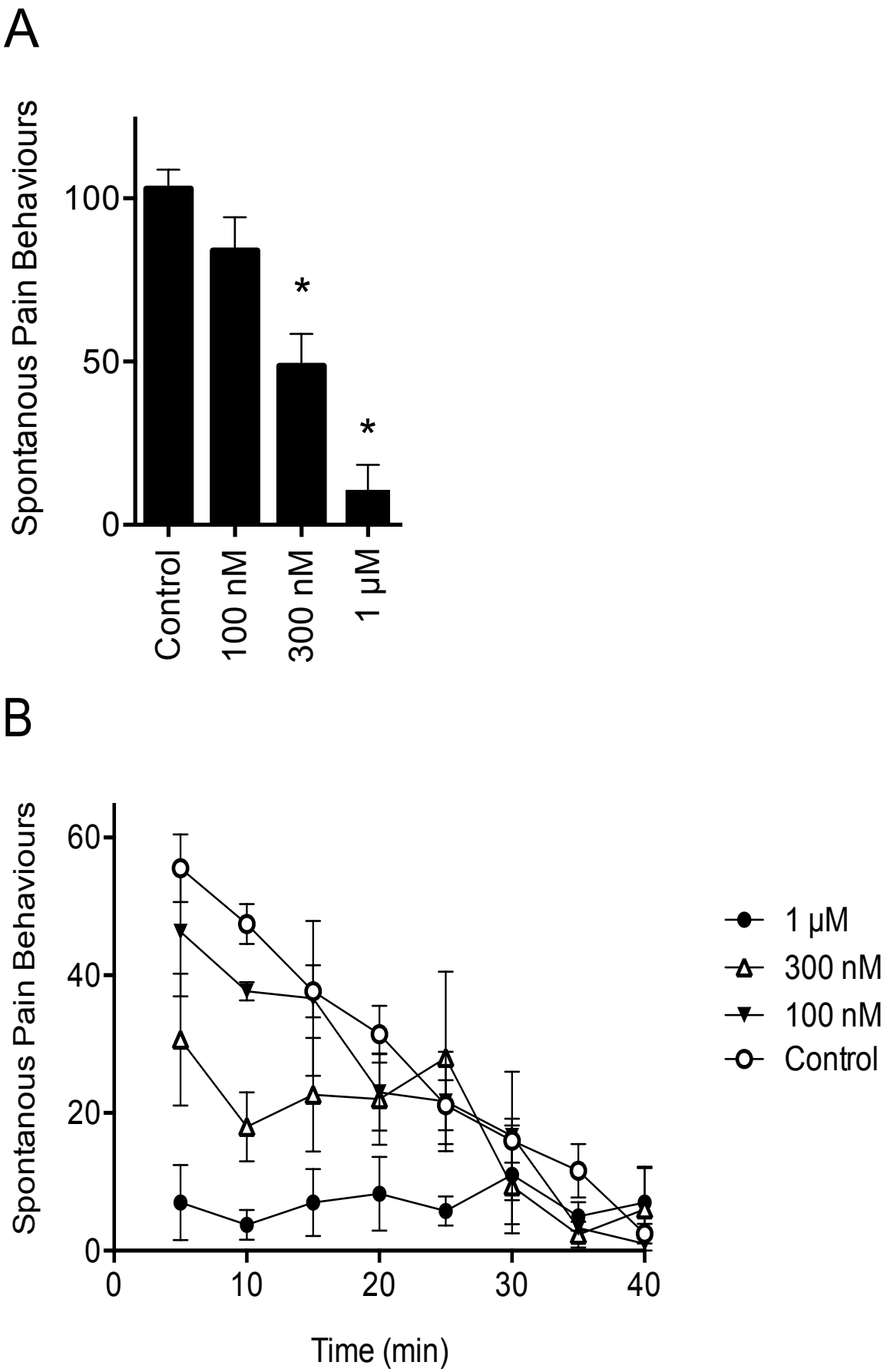
A
Spontanous Pain Behaviours
100
50
0
*
*
Control
100 nM
300 nM
1 µM
B
Spontanous Pain Behaviours
60
40
20
0
0
10
20
30
40
Time (min)
1 µM
300 nM
100 nM
Control

Figure 10

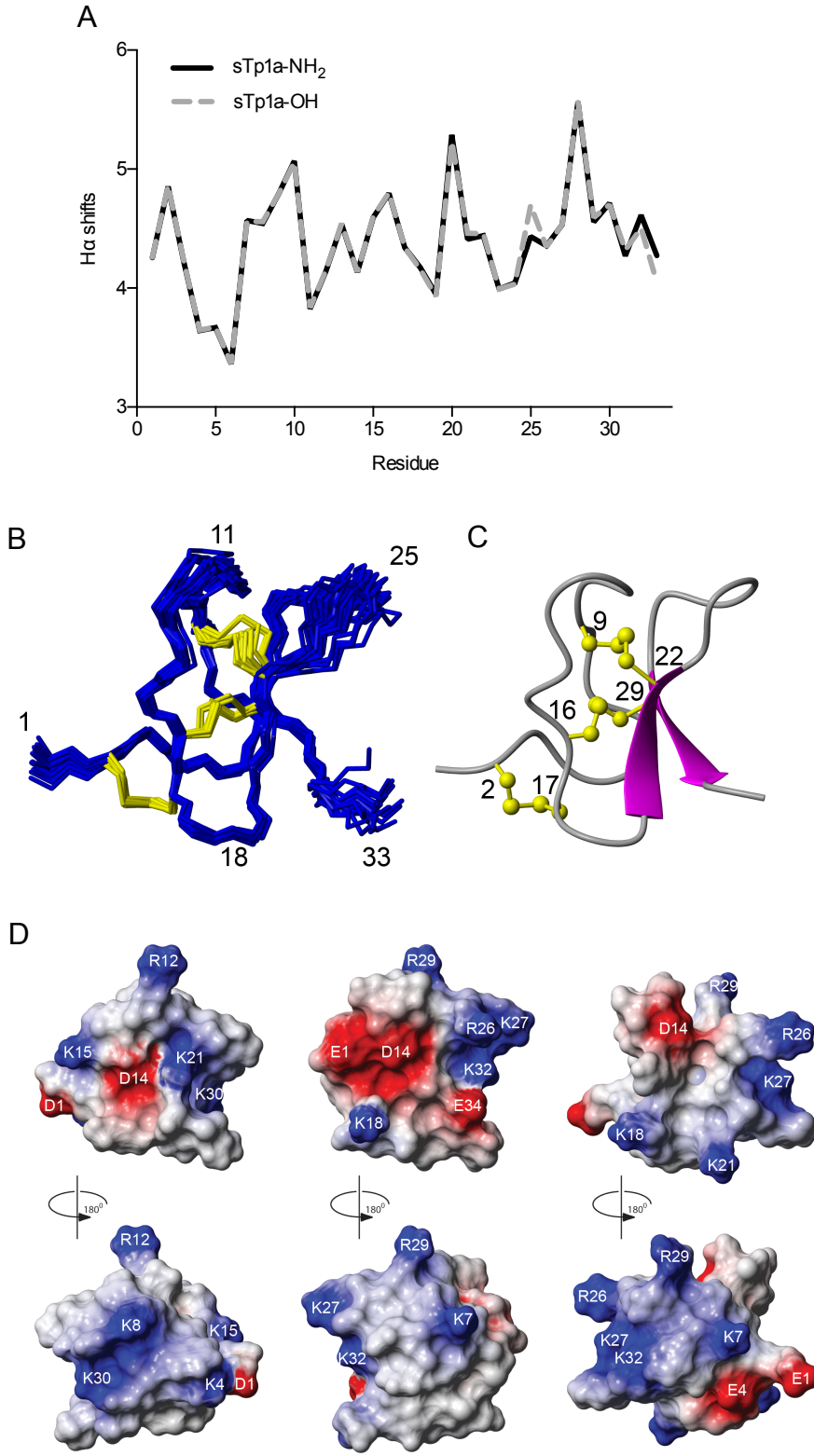
A
sTp1a-NH2
sTp1a-OH
Hα shifts
Residue
B
11
25
1
18
33
C
9
22
29
16
2
17
D
R12
K15
K21
D14
D1
K30
R29
R26
K27
E1
D14
K32
E34
K18
R29
D14
R26
K27
K18
K21
180°
R12
K8
K15
K30
K4
D1
R29
K27
K7
K32
R29
R26
K27
K32
K7
E4
E1

Figure 11